



Comparison of water vapor measurements by airborne Sun photometer and near-coincident in situ and satellite sensors during INTEX/ITCT 2004

J. Livingston,¹ B. Schmid,^{2,3} J. Redemann,² P. B. Russell,⁴ S. A. Ramirez,² J. Eilers,⁴ W. Gore,⁴ S. Howard,² J. Pommier,² E. J. Fetzer,⁵ S. W. Seemann,⁶ E. Borbas,⁶ D. E. Wolfe,⁷ and A. M. Thompson⁸

Received 3 July 2006; revised 8 December 2006; accepted 12 February 2007; published 6 June 2007.

[1] We have retrieved columnar water vapor (CWV) from measurements acquired by the 14-channel NASA Ames Airborne Tracking Sun photometer (AATS-14) during 19 Jetstream 31 (J31) flights over the Gulf of Maine in summer 2004 in support of the Intercontinental Chemical Transport Experiment (INTEX)/Intercontinental Transport and Chemical Transformation (ITCT) experiments. In this paper we compare AATS-14 water vapor retrievals during aircraft vertical profiles with measurements by an onboard Vaisala HMP243 humidity sensor and by ship radiosondes and with water vapor profiles retrieved from AIRS measurements during eight Aqua overpasses. We also compare AATS CWV and MODIS infrared CWV retrievals during five Aqua and five Terra overpasses. For 35 J31 vertical profiles, mean (bias) and RMS AATS-minus-Vaisala layer-integrated water vapor (LWV) differences are -7.1% and 8.8% , respectively. For 22 aircraft profiles within 1 hour and 130 km of radiosonde soundings, AATS-minus-sonde bias and RMS LWV differences are -5.4% and 10.7% , respectively, and corresponding J31 Vaisala-minus-sonde differences are 2.3% and 8.4% , respectively. AIRS LWV retrievals within 80 km of J31 profiles yield lower bias and RMS differences compared to AATS or Vaisala retrievals than do AIRS retrievals within 150 km of the J31. In particular, for AIRS-minus-AATS LWV differences, the bias decreases from 8.8% to 5.8% , and the RMS difference decreases from 21.5% to 16.4% . Comparison of vertically resolved AIRS water vapor retrievals (LWV_A) to AATS values in fixed pressure layers yields biases of -2% to $+6\%$ and RMS differences of $\sim 20\%$ below 700 hPa. Variability and magnitude of these differences increase significantly above 700 hPa. MODIS IR retrievals of CWV in 205 grid cells (5×5 km at nadir) are biased wet by 10.4% compared to AATS over-ocean near-surface retrievals. The MODIS-Aqua subset (79 grid cells) exhibits a wet bias of 5.1% , and the MODIS-Terra subset (126 grid cells) yields a wet bias of 13.2% .

Citation: Livingston, J., et al. (2007), Comparison of water vapor measurements by airborne Sun photometer and near-coincident in situ and satellite sensors during INTEX/ITCT 2004, *J. Geophys. Res.*, 112, D12S16, doi:10.1029/2006JD007733.

1. Introduction

[2] During July and August 2004, a twin turboprop Jetstream 31 (J31) flew 19 science flights over the Gulf of

Maine in support of the International Consortium for Atmospheric Research on Transport and Transformation (ICARTT [*Fehsenfeld et al.*, 2006]) effort to quantify the air quality, intercontinental transport, and radiative energy budgets in air masses moving across the US and over the Atlantic Ocean to Europe. ICARTT included Phase A of the Intercontinental Chemical Transport Experiment (INTEX-A [*Singh et al.*, 2006]) and the Intercontinental Transport and Chemical Transformation (ITCT [*Fehsenfeld et al.*, 2006]) experiment. The goal of the J31 flights was to characterize aerosol, water vapor, cloud, and ocean surface radiative properties and effects in flights that sampled polluted and clean air masses in coordination with measurements from other aircraft, a ship, and various satellites. Specific science objectives of the J31 included validating satellite retrievals of aerosol optical depth (AOD) spectra and of water vapor

¹SRI International, Menlo Park, California, USA.

²Bay Area Environmental Research Institute, Sonoma, California, USA.

³Now at Pacific Northwest National Laboratory, Richland, Washington, USA.

⁴NASA Ames Research Center, Moffett Field, California, USA.

⁵Jet Propulsion Laboratory, California Institute of Technology, Pasadena, California, USA.

⁶Cooperative Institute for Meteorological Satellite Studies, University of Wisconsin, Madison, Wisconsin, USA.

⁷Earth System Research Laboratory, NOAA, Boulder, Colorado, USA.

⁸Meteorology Department, Pennsylvania State University, University Park, Pennsylvania, USA.

columns, as well as measuring aerosol effects on radiative energy fluxes.

[3] The primary instruments on the J31 were the 14-channel NASA Ames Airborne Tracking Sun photometer, AATS-14 [Schmid *et al.*, 2000, 2003a, 2003b], and an upward and downward looking pair of solar spectral flux radiometers. Other instrumentation included a Vaisala HMP243 humidity sensor and other instruments to provide basic meteorological and navigational information. J31 flight patterns included a mixture of vertical profiles (spiral and ramped ascents and descents) and constant altitude horizontal transects at a variety of altitudes. In most cases, flights were designed to include a near sea surface horizontal transect in a region of minimal cloud cover during or near the time of an Aqua and/or Terra satellite overpass, in addition to a low-altitude flyby and vertical profile above the NOAA Research Vessel *Ronald H. Brown*. AATS-14 measurements of the relative intensity of the direct solar beam allow retrieval of aerosol optical depth (AOD) at 13 wavelengths in addition to columnar water vapor (CWV). The quantity CWV equals the amount of water vapor in the vertical column of unit cross-sectional area above the aircraft, and, for ground-based measurements, equals the total precipitable water vapor (TPW). Data obtained during suitable aircraft ascents and descents can be differentiated to yield vertical profiles of aerosol extinction and water vapor density (ρ_w).

[4] Because water vapor is the primary gaseous absorber of infrared radiation in the atmosphere, knowledge of its horizontal and vertical distribution is critical to understanding its effect on the Earth's climate. Fortunately, continuous global measurements of the distribution of water vapor are now being acquired by satellite sensors such as the Moderate Resolution Imaging Spectroradiometer (MODIS [Kaufman *et al.*, 1997]) on Aqua and Terra, the Atmospheric Infrared Sounder (AIRS [Aumann *et al.*, 2003]) instrument suite on Aqua, and the Tropospheric Emission Spectrometer (TES [Beer, 2006]) on Aura. While only satellite sensors can provide a global view, there remains a critical need for continuing validation of the satellite products by information from sensors with superior measurement capabilities. Existing international networks of radiosondes and ground-based Sun photometers (AERONET [Holben *et al.*, 1998]), and lidars and microwave radiometers at selected land sites (e.g., the Atmospheric Radiation Measurement Southern Great Plains [ARM-SGP] site) are available and can be used to validate satellite water vapor retrievals over land [e.g., Whiteman *et al.*, 2006; Tobin *et al.*, 2006]. However, validation of satellite over-ocean water vapor retrieval algorithms generally must rely on a combination of sparse radiosonde or remote measurements and numerical model outputs. This is a role for which AATS-14 and the J31 are well suited. Previous studies [Schmid *et al.*, 2000, 2003a, 2006] have compared AATS-14 retrievals of CWV and ρ_w over land and over ocean with coincident aircraft-based in situ and/or ground-based remote measurements. This paper compares AATS-14 over-ocean water vapor retrievals with simultaneous in situ water vapor measurements by the J31 Vaisala sensor and with temporally and spatially near-coincident measurements from radiosondes released from the *Ronald H. Brown*, and it extends the comparisons to corresponding water vapor retrievals by MODIS and by

AIRS. In other papers dealing with AATS-14 measurements acquired during INTEX/ITCT, Russell *et al.* [2007] discuss the AATS-14 AOD measurements and comparisons to MODIS and to MISR (Multiangle Imaging Spectroradiometer [Diner *et al.*, 1998, Martonchik *et al.*, 1998]), and Redemann *et al.* [2006] present the J31 measurements of aerosol effects on radiative energy fluxes.

2. Data Sources

2.1. Airborne Sun Photometer

[5] The NASA Ames Airborne Tracking Sun photometer (AATS-14) measures the relative intensity of the direct solar beam in 14 spectral channels with center wavelengths ranging from 354 to 2138 nm and full width at half maximum (FWHM) bandwidths of ~ 5 nm (exceptions are 2.0 nm for the 354-nm channel and 17.3 nm for the 2138-nm channel). The data acquisition system samples at 3 Hz, and every 4 s it records detector voltages consisting of an average and standard deviation of nine samples taken during the first 3 of the 4 s. These data are stored together with data on instrument tracking and temperature control, aircraft location, and ambient temperature, relative humidity, and static pressure. The standard deviations of all channels are used subsequently in a cloud-screening algorithm, as described by Schmid *et al.* [2003b]. Data are transmitted serially from a computer within the instrument to a remote operator station (laptop computer). The science data are then combined with previously determined radiometric calibration values to calculate and display aerosol optical depth (AOD) and columnar water vapor in real time at the operator station. For more information on the instrument and its mounting on the J31, see the companion paper by Russell *et al.* [2007].

[6] Our methods for data reduction, calibration, and error analysis have been described in detail previously [Russell *et al.*, 1993a, 1993b; Schmid and Wehli, 1995; Schmid *et al.*, 1996, 1998, 2001, 2003b]. The AATS-14 channels have been chosen to permit separation of total (path-integrated) aerosol, water vapor, and (for measurements acquired at large solar zenith angles, SZA, with small AOD [Livingston *et al.*, 2005]) ozone attenuation along the slant path from the Sun to the instrument. In practice, the measured detector voltages are combined with separately determined (see following paragraph) exoatmospheric detector voltages, $V_0(\lambda)$, to yield slant-path transmissions. From these slant-path transmissions we retrieve AOD in 13 narrow wavelength bands centered between 354 and 2139 nm and CWV from the channel centered at 941 nm. Because almost all measurements acquired during INTEX/ITCT were for $SZA \leq 40^\circ$, we use ozone total column amounts from TOMS satellite retrievals and adjust these values for the J31 altitude using the 1976 standard ozone model vertical distribution. Rayleigh scattering corrections use the Bucholtz [1995] cross sections and static pressure measured on the J31. As described by Russell *et al.* [2007], measurements in some AATS-14 channels also require corrections for gas absorption (NO_2 , H_2O , $\text{O}_2\text{-O}_2$, CH_4 , N_2O , and CO_2) in order to retrieve AOD.

[7] AATS-14 was calibrated by analysis of sunrise measurements acquired at Mauna Loa Observatory (MLO), Hawaii, in June 2004 before the ITCT deployment and also

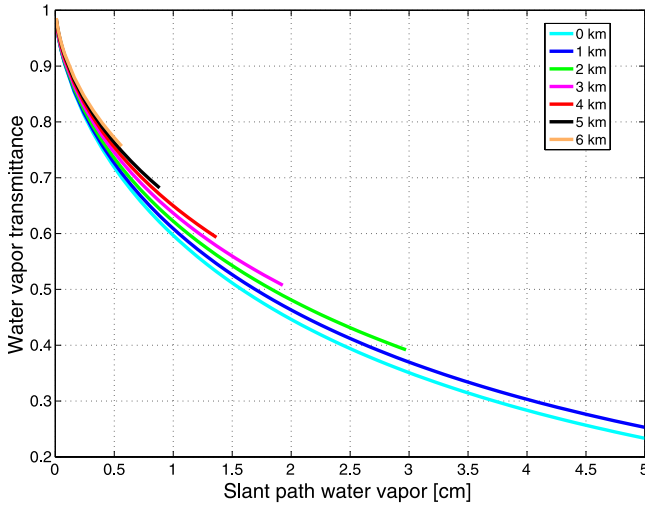


Figure 1. LBLRTM calculations of water vapor transmittance T_w as a function of slant path water vapor and aircraft altitude for the AATS-14 941-nm channel.

by analysis of sunset measurements acquired on four dedicated J31 flights (29 July and 2, 7, and 8 August) during the experiment. The $V_0(\lambda)$ were derived using the Langley plot technique [e.g., *Russell et al.*, 1993a, 1993b; *Schmid and Wehrli*, 1995] for all channels except 941 nm, for which a modified Langley technique was employed to account for water vapor absorption [*Reagan et al.*, 1995; *Michalsky et al.*, 1995; *Schmid et al.*, 1996, 2001]. Mean values of $V_0(\lambda)$ obtained during the four ITCT calibration flights agreed with the premission MLO mean values to $\leq 0.5\%$ in all channels except 519 nm and 1240 nm, where differences were 0.7% and 1.3%, respectively. In the 941-nm channel, mean values agreed to within 0.4%. For measurements acquired prior to the first airborne calibration on 29 July, we assumed a linear temporal variation in $V_0(\lambda)$ between the mean MLO premission and mean airborne calibration constants; for measurements acquired after 29 July, the mean airborne constants were used. For all channels except 941 nm, standard deviations in the calculated V_0 values ranged from $<0.1\%$ to 0.3% for the MLO measurements, and from $<0.1\%$ to 0.8% for the airborne measurements. Corresponding standard deviations in V_0 in the 941-nm channel were 1.8% for the MLO data and 1.1% for the airborne measurements. These standard deviations have been included as the statistical component of the total uncertainty in $V_0(941 \text{ nm})$. For ITCT near-surface CWV retrievals, the calculated uncertainty in $V_0(941 \text{ nm})$ contributes 0.07–0.10 g/cm^2 ($\sim 3\text{--}4\%$ of the CWV) to the total CWV uncertainty (computed following *Schmid et al.* [1996]). This amount represents $\sim 50\%$ of the total calculated uncertainty in CWV. The other sources of error in CWV are the uncertainty in the spectroscopic model parameterization of the water vapor transmittance (see below) and the uncertainty in AOD.

[8] Because absorption by water vapor varies strongly within the 5-nm FWHM band pass of the AATS-14 channel centered at 941 nm, the usual Beer-Lambert-Bouguer expression must be modified to correctly describe the relationship between the incoming directly transmitted solar

irradiance and the output detector voltage, $V(941)$, within that channel. In particular,

$$V(941 \text{ nm}) = V_0(941 \text{ nm}) d^{-2} \exp \left[- \sum_i m_i \tau_i(941 \text{ nm}) \right] T_w, \quad (1)$$

where $V_0(941 \text{ nm})$ is the exoatmospheric voltage constant, d is the Earth-Sun distance in astronomical units at the time of observation, $\tau_i(941 \text{ nm})$ is the spectral optical depth due to aerosol extinction, Rayleigh scattering, or ozone absorption, and T_w is the band- and source-weighted water vapor transmittance. In our analysis of the AATS-14 INTEX/ITCT data set, we employed an expression analogous to that of the three-parameter expression of *Ingold et al.* [2000] for parameterizing the water vapor transmittance, T_w :

$$T_w = c \exp(-aw_s^b), \quad (2)$$

where w_s is the amount of water vapor along the slant path and is in units of g/cm^2 (or typical precipitable water vapor units of cm, since the mean liquid water density = 1 g/cm^3), and the coefficients a , b and c are least squares fitting parameters determined by executing a radiative transfer model over a range of slant path water vapor amounts. For $c = 1$, equation (2) is equivalent to the two-parameter expression of *Bruegge et al.* [1992]. Strictly speaking, as noted by *Ingold et al.* [2000], this equation only applies for $w_s > 0$ to avoid the nonphysical result for $c \neq 1$ at vanishing water vapor absorption ($w_s = 0$). Subsequent modeling and calculation of the water vapor relative optical air mass, m_{H_2O} , which is the ratio of the integrated amount of water vapor along the vertical to the integrated amount along the slant path, then permits calculation of the CWV from the slant path water vapor

$$w_s = m_{H_2O} \text{ CWV}. \quad (3)$$

[9] In practice, we applied the two- and three-parameter expressions separately to results from LBLRTM_V9.2 [*Clough et al.*, 2005] runs for a wide range of solar zenith angles (i.e., air masses) and the 6 built-in standard atmospheres at aircraft (AATS) altitudes every 1 km between the surface and 8 km. For altitudes below 4 km, results for the two- and three-parameter fits to the LBLRTM calculations yielded RMS errors that were within 0.2% of each other, so we used the two-parameter fits at altitudes 0–3 km, and the three-parameter fits at altitudes 4–8 km. The results for altitudes ≤ 6 km are shown in Figure 1 for slant water paths measured during INTEX-ITCT, and the fitting coefficients are listed in Table 1. Figure 1 shows that a calculation of CWV that ignores the instrument altitude can result in an incorrect determination of slant path (hence columnar) water vapor. In particular, if it is assumed that the instrument is located at sea level, then CWV would be underestimated for altitudes above sea level, and the errors would be greatest for large SZA (high air mass values), and high CWV (hence high slant water vapor) amounts. For most data presented in this paper, $\text{SZA} \leq 40^\circ$, corresponding to air mass values ≤ 1.3 . As will be shown in Figure 2 below, typical CWV values measured by AATS during ITCT at

Table 1. Coefficients of *Ingold et al.* [2000] Three-Parameter Functional Fit (Two-Parameter at Altitudes Below 4 km) to LBLRTM_v9.2 Calculations of Water Vapor Transmittance as a Function of Slant Path Water Vapor w_s for the AATS-14 Channel Centered at 940.6 nm^a

Altitude, km	a	b	c
0	0.51623	0.6439	1.00000
1	0.49669	0.6331	1.00000
2	0.47492	0.6238	1.00000
3	0.45191	0.6186	1.00000
4	0.43700	0.6053	1.00540
5	0.42217	0.5929	1.00924
6	0.40499	0.5859	1.01006
7	0.38888	0.5892	1.00855
8	0.38005	0.6059	1.00614

^aUnit of w_s is cm or g/cm².

aircraft altitudes of 1 km and 2 km were 1.0–2.0 g/cm² and 0.5–1.0 g/cm², respectively. For these CWV amounts and aircraft altitudes and for an air mass of 1.3, the errors in calculated CWV that would result from not accounting for the altitude of the measurement are ~ 0.06 – 0.14 g/cm² (6–7%) at 1 km and ~ 0.05 – 0.12 g/cm² (11–12%) at 2 km. At higher altitudes absolute errors would decrease (and relative errors would increase) because the amount of CWV above the aircraft decreases rapidly with altitude within the first few km above the surface. This altitude-dependent parameterization of water vapor transmittance as a function of slant water vapor amount represents a more realistic and rigorous treatment of airborne measurements than the single altitude parameterization that we have used in previous studies [e.g., *Schmid et al.*, 2003b; *Redemann et al.*, 2003], for which it was assumed that the uncertainty in AATS CWV due to the single altitude parameterization was 0.1 g/cm².

[10] Using the water vapor transmittance parameterization described above, we calculated CWV from the values of the solar transmittance calculated from measurements in the AATS 941-nm channel. Vertical differentiation of the CWV measurements acquired during aircraft ascent or descent then yields a profile of ρ_w . In practice, we used the smoothing methodology of *Schmid et al.* [2000] to calculate ρ_w . This involves averaging the CWV profile within thin altitude bins (we used 20–50 m bins for this study), then fitting a smoothing spline to the averaged profile, and finally differentiating the spline fit. It is necessary to smooth the CWV profile before differentiation to eliminate AATS-measured increases in CWV with height. Such increases are not possible in a horizontally homogeneous, time-invariant atmosphere. However, as noted by *Schmid et al.* [2003a], in the real atmosphere they can occur because (1) the Sun photometer can only measure the transmittance along the Sun photometer-to-Sun path; (2) that path in general passes through a horizontally inhomogeneous, time-varying atmosphere; and (3) the path and the atmosphere move with respect to each other because of aircraft movement and horizontal advection. To avoid over-smoothing at altitudes that exhibit real variations of CWV we occasionally allow the ρ_w to become slightly negative.

2.2. J31 Vaisala Humidity Sensor

[11] Relative humidity was measured by a Vaisala HUMICAP Dewpoint Transmitter HMP243, which consists of

two probes: a heated composite humidity HUMICAP sensor and an optional temperature head, that were mounted beneath the cockpit on the lower right side of the J31 fuselage. Total and static atmospheric pressure were measured by separate Setra Model 470 pressure sensors mounted on the J31. Prior to the ITCT deployment, both pressure sensors were calibrated in the laboratory at NASA Ames. Calibration of the Vaisala HMP243, which was purchased and mounted on the J31 in late spring 2004, was provided by Vaisala.

[12] Both Vaisala sensor probes mounted on the J31 are subject to dynamic heating effects due to the motion of the aircraft. The static temperature, T_{static} , of the ambient atmosphere is calculated from the output, T_{total} , of the Vaisala temperature probe by

$$T_{\text{static}} = T_{\text{total}} \left(\frac{P_{\text{static}}}{P_{\text{total}}} \right)^{\left(\frac{k-1}{k} \right)}, \quad (4)$$

where $k = 1.4$ is the ratio of specific heats for water vapor, $\left(\frac{c_p}{c_v} \right)$. The quantity, $\text{RH}_{\text{Vaisala}}$, output by the Vaisala humidity sensor can be written as

$$\text{RH}_{\text{Vaisala}} = 100 * \left(\frac{e_{\text{true}}}{e_{\text{sat}}(T_{\text{total}})} \right), \quad (5)$$

where e_{true} is the true water vapor pressure, and $e_{\text{sat}}(T_{\text{total}})$ is the saturation vapor pressure at temperature T_{total} . It follows that the true ambient relative humidity is just

$$\text{RH}_{\text{true}} = \text{RH}_{\text{Vaisala}} * \left(\frac{e_{\text{sat}}(T_{\text{total}})}{e_{\text{sat}}(T_{\text{static}})} \right), \quad (6)$$

where the saturation vapor pressures at temperatures T_{total} and T_{static} are calculated using the formulae provided in the Vaisala instrument manual. The measured profiles of relative humidity, temperature, and pressure obtained during J31 ascents and descents have been converted to corresponding profiles of water vapor density (absolute humidity) using the approximate equation of *Bögel* [1977]. Integration of these profiles yields the amount of water vapor (LWV) in the layer between the bottom and the top of the J31 profile. The uncertainty in calculated water vapor density has been estimated by interpolation within the Vaisala HMP240 User's Guide table that gives the accuracy of calculated absolute humidity as a function of the measured ambient temperature and relative humidity. These uncertainties have been propagated through the integral over altitude to yield an estimate of the corresponding uncertainty in LWV.

2.3. Ship Radiosondes

[13] Vaisala RS92 SGP radiosondes were launched regularly from the *Ronald H. Brown* during summer 2004 in support of the combined NEAQS (New England Air Quality Study)–ITCT 2004 study. Vaisala RS80 radiosondes attached to ENSCI ozonesondes were released daily at ~ 1500 UT from the *Ronald H. Brown* in support of IONS (INTEX Ozonesonde Network Study; *Thompson et al.* [2007]). We have converted the radiosonde-measured profiles of relative humidity, temperature, and pressure to

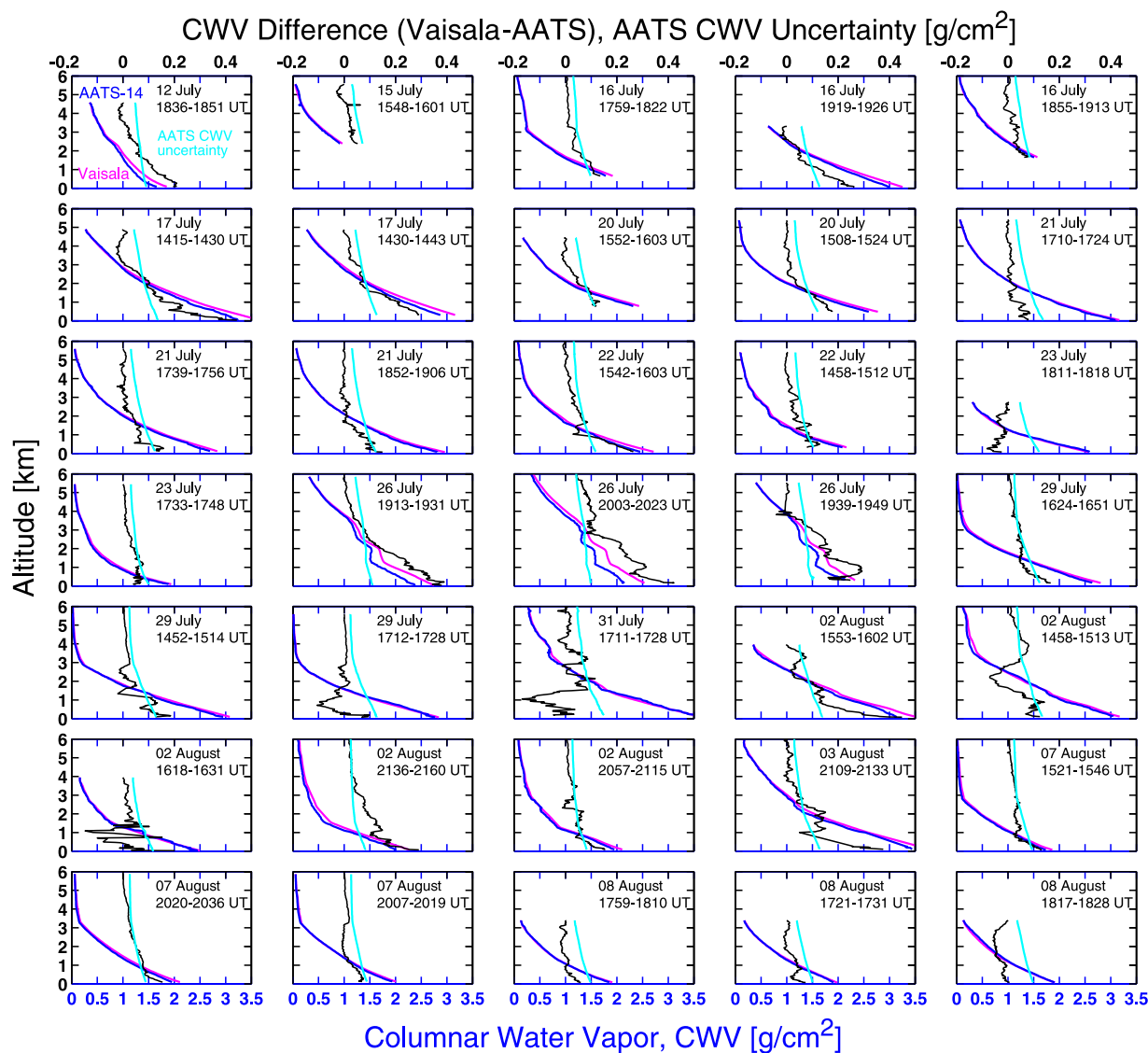


Figure 2. Vertical profiles of CWV calculated from measurements by AATS-14 (blue) and the J31 Vaisala HMP243 (magenta) during INTEX-A/ITCT 2004. Vaisala values have been set equal to the AATS CWV at the top of each profile. The cyan line is the uncertainty in AATS-14 CWV, and the black line shows the Vaisala-minus-AATS CWV difference.

corresponding profiles of water vapor density using Bögel [1977]. Integration of these profiles yields the amount of water vapor in the column (layer) bounded by the upper and lower altitudes of the sonde data. Section 3.1 compares J31 AATS-14 and Vaisala water vapor profile results with corresponding values calculated from near-coincident measurements acquired by 42 RS92 and 4 RS80 radiosondes launched from the *Ronald H. Brown*. Quantifying the uncertainty in the sonde-inferred water vapor is not straightforward, and we do not attempt to do so here. A recent study by Miloshevich *et al.* [2006] examines the mean accuracy and variability of radiosonde water vapor measurements relative to simultaneous measurements from the University of Colorado Cryogenic Frostpoint Hygrometer (CFH) at the ARM SGP site. They conclude “there is no simple answer to the question ‘how accurate are water vapor measurements from a given radiosonde type?’” Nevertheless, they report

that the RS92 was the most accurate of the radiosondes tested and that, for nighttime RS92 measurements uncorrected for time lag or empirical calibration, its mean percentage accuracy relative to the CFH reference sensor was <5% for most conditions in the lower troposphere. The absolute accuracy of the CFH sensor was found to be about 3% in the lower troposphere. Daytime RS90 measurements are also subject to a dry bias due to solar radiation effects.

2.4. MODIS

[14] The Moderate Resolution Imaging Spectroradiometer (MODIS) is a scanning spectroradiometer with 36 visible, near-infrared, and infrared spectral bands between 0.553 and 14.235 μm [King *et al.*, 1992]. There are two MODIS instruments currently in operation: one on Terra, which was launched in December 1999, and one on Aqua, which was launched in May 2002. The operational MODIS algorithm

for retrieving atmospheric temperature and moisture distributions, total column ozone burden, and integrated TPW from MODIS infrared radiances has been described in detail by *Seemann et al.* [2003]. In particular, water vapor mixing ratio is retrieved at 101 fixed pressure levels from the clear-sky radiances measured in the 11 MODIS infrared bands between 4.482 and 14.385 μm within a 5×5 pixel field of view (approximately 5-km resolution at nadir) over land and ocean for both day and night. TPW is then calculated by integrating over the 101 levels. In fact, MODIS does not have high enough spectral resolution to yield independent information at that many vertical levels, so the archived MODIS Level 2 atmospheric profile product (MOD07_L2 for MODIS-Terra, and MYD07_L2 for MODIS-Aqua) includes retrieval results at only 20 atmospheric pressure levels, in addition to TPW. All MODIS water vapor products used in this paper were derived from integration of the 101-level retrievals from the most recent version, V5.2, of the MODIS IR retrieval algorithm. There is a separate MODIS algorithm [*Gao and Kaufman*, 2003] that uses data measured at 1-km resolution in five near-infrared MODIS channels centered between 0.865 and 1.24 μm to derive TPW during daytime over clear land areas, over the extended glint area over clear ocean areas, and above clouds over both land and ocean. These data are not considered in this paper because our measurements focused on cloud-free locations outside the MODIS glint over the Gulf of Maine. Terra and Aqua are Sun-synchronous satellites, with Terra's sunlit overpasses occurring in the local morning and Aqua's in the local afternoon. Local equator crossing times for Terra and Aqua are ~ 1030 and ~ 1330 LT, respectively. Both MODIS water vapor products are particularly well suited for measuring spatial variability in column water vapor because of their high spatial resolution.

2.5. AIRS

[15] The Atmospheric Infrared Sounder (AIRS) experiment actually consists of three separate instruments on the Aqua satellite. AIRS was designed to obtain continuous global measurements of the Earth's atmospheric water vapor and temperature profiles. The AIRS instrument is a hyperspectral nadir cross-track scanning infrared spectrometer with a 15 km field of view (FOV) [*Pagano et al.*, 2003]. Also on Aqua are two multichannel microwave sounders: the Advanced Microwave Sounding Unit (AMSU-A) with a 45 km FOV and the Humidity Sounder for Brazil (HSB) with a 15 km FOV [*Lambrigtsen*, 2003; *Lambrigtsen and Calheiros*, 2003]. Both AIRS and AMSU-A continue to operate, but the HSB ceased operation in early February 2003 because of a mirror scan motor failure. AIRS geophysical retrievals [*Susskind et al.*, 2003, 2006; *Aumann et al.*, 2003] use the infrared and the microwave measurements. Like AIRS, the AMSU-A is also a cross-track scanner, but it scans three times as slowly as AIRS (once per 8 s) and its footprints are approximately three times as large as those of AIRS (45 km at nadir). These differences result in three AIRS scans per AMSU-A scan and nine AIRS footprints per AMSU-A footprint. AIRS data retrievals are generated at the nominal 45-km nadir resolution of the AMSU in granules, which consist of 45 cross-track scans of the AMSU-A mirror. Each scan consists of 30 contiguous AMSU FOVs. The relatively coarse horizontal resolution of

the AIRS retrievals prevents comparing them to the fine-scale horizontal structure (e.g., gradients) measured by AATS within a typical J31 transect. However, the AIRS retrievals are unique in providing measurements of the vertical distribution of water vapor at a resolution of 1–2 km in altitude. In this paper, we include only data extracted from the AIRS high vertical resolution (100 pressure levels) Version 4.0 L2 Support Atmospheric/Surface Product files. Additional details on instrument and data acquisition specifications for the AIRS instrument suite can be found in the AIRS/AMSU/HSB Version 4.0 Data Release User Guide [*Olsen et al.*, 2005a; *Aumann et al.*, 2003].

3. Results and Discussion

3.1. Comparison of AATS Water Vapor Retrievals With Coincident J31 Vaisala HPM243 Measurements and With Near-Coincident Ship Balloonsonde Measurements

[16] In this section we compare AATS-14 water vapor retrievals with coincident J31 Vaisala HPM243 measurements acquired during 35 aircraft vertical profiles, and we also compare AATS-14 and J31 Vaisala retrievals with near-coincident measurements acquired by 46 radiosondes launched from the *Ronald H. Brown*.

[17] Figure 2 overplots profiles of CWV and CWV differences calculated from AATS-14 and J31 Vaisala measurements obtained during 35 separate J31 ascents and descents. Uncertainties in AATS-derived CWV are shown on the same scale (top) as the CWV differences. Because the J31 Vaisala cannot measure CWV above the J31 altitude, each Vaisala CWV profile has been set equal to the AATS-14 CWV value at the top of the profile. The units of CWV are g/cm^2 or, equivalently, cm, the typical units of precipitable water vapor. Minimum near-surface CWV values were $\sim 1.9 \text{ g}/\text{cm}^2$, and maximum values were $\sim 3.6 \text{ g}/\text{cm}^2$. AATS CWV absolute uncertainties decrease with altitude from $\sim 0.15 \text{ g}/\text{cm}^2$ (for the maximum calculated CWV) at the bottom of the profile to $\sim 0.02 \text{ g}/\text{cm}^2$ at 6.0 km. In general, Vaisala CWV exceeds AATS CWV. The Vaisala-minus-AATS CWV differences generally increase below 2 km, with the largest differences of $\sim 0.4 \text{ g}/\text{cm}^2$ at the J31 minimum altitude ~ 50 m above the ocean. One plausible explanation for these differences is the difference in the remote and in situ measurement techniques. The basic atmospheric parameter derived from any AATS measurement is a slant path-integrated attenuation that can then be converted to a height-integrated quantity by assuming horizontal homogeneity of the overlying attenuator. For AATS-14, each derived CWV value represents a relatively short (3-s average) temporal snapshot of the total amount of water vapor in the column above the aircraft. In contrast, the J31 Vaisala measures a height-specific relative humidity, from which absolute humidity can be calculated. Calculation of CWV above a particular altitude from the Vaisala data requires integrating the Vaisala-measured water vapor density profile from that altitude to the top of the J31 profile and then adding the amount of CWV measured by AATS at the top of the profile. Because the J31 took 7 to 24 min to complete each profile shown in Figure 2, each Vaisala CWV value actually includes data sampled over a much wider range of times and aircraft locations than does the

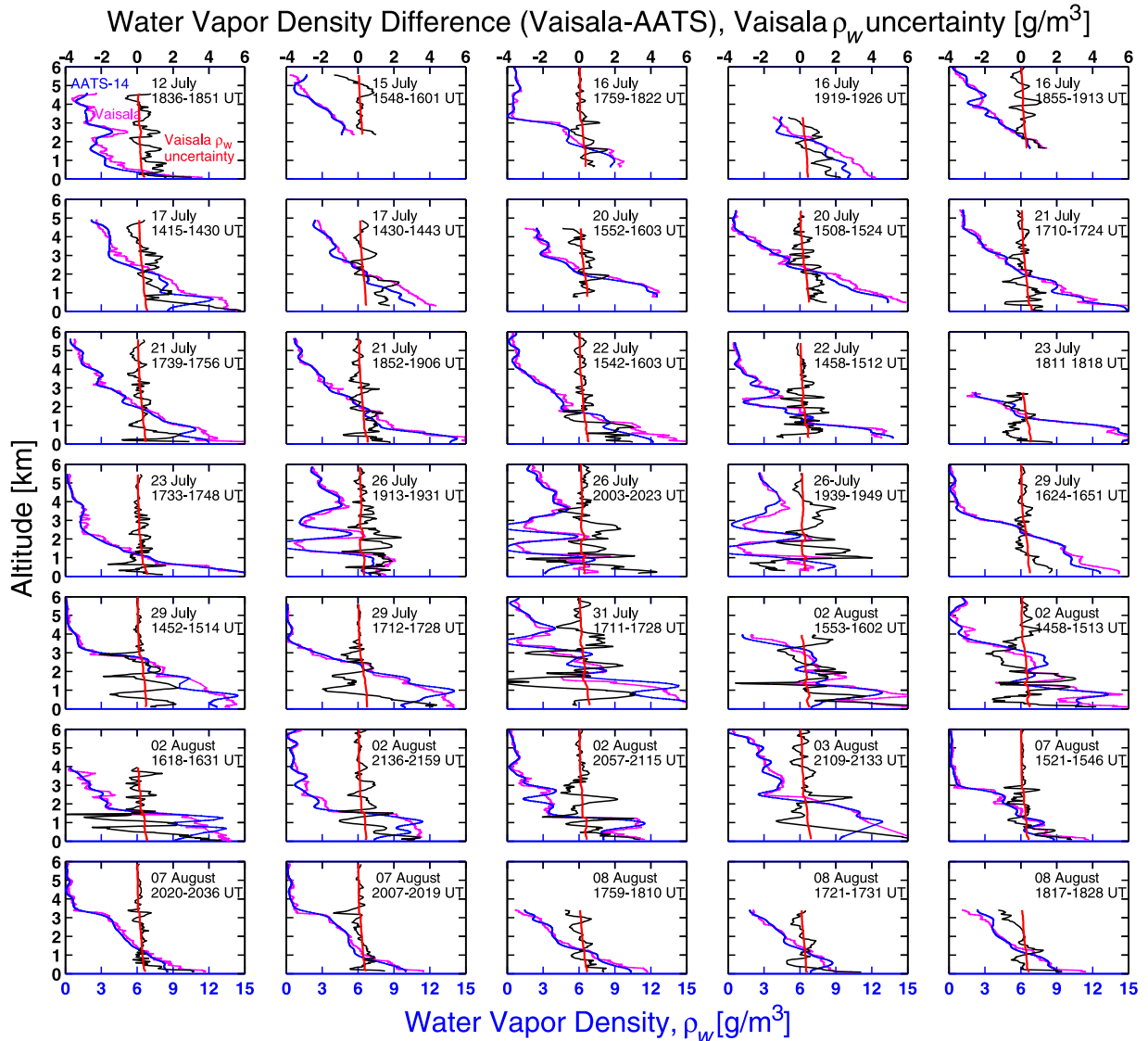


Figure 3. Vertical profiles of AATS-14 (blue) and J31 Vaisala (magenta) water vapor density, ρ_w , for the profiles shown in Figure 2. The red line is the uncertainty in the Vaisala ρ_w , and the black line shows the Vaisala-minus-AATS ρ_w differences.

corresponding AATS CWV value. Hence the difference between the AATS 3-s CWV and the Vaisala time- and space-integrated CWV at a specific altitude includes temporal and/or spatial atmospheric differences (in addition to any differences in measurement technique, calibration, etc.).

[18] Figure 3 overplots profiles of water vapor density, ρ_w , and ρ_w differences calculated from J31 Vaisala and AATS-14 measurements for the same J31 profiles shown in Figure 2. The uncertainties $\delta\rho_w$ in the Vaisala ρ_w are shown on the same scale (top) as the differences. For clarity, the estimated uncertainties in AATS ρ_w are not shown, but, with a few exceptions, they are comparable to the Vaisala $\delta\rho_w$. Because of the nature of the remote measurement that includes temporal and spatial atmospheric variability and requires some vertical smoothing, the AATS-14 ρ_w retrieval cannot yield the fine vertical resolution provided by the in situ J31 measurement. This is reflected both in the ρ_w difference profiles and in the comparison of these

differences with the Vaisala $\delta\rho_w$. Water vapor horizontal and/or temporal inhomogeneities can lead to AATS measurements of increasing CWV with altitude and result in physically implausible (i.e., negative) retrievals of water vapor density at specific altitudes, as can be seen, for example, in the profiles for 26 July in Figure 3. Additional vertical smoothing would eliminate these negative retrievals, but at a cost of reduced vertical resolution that would essentially discard useful profile information. Hence there is a tradeoff between vertical resolution and accuracy of the AATS ρ_w profiles. The optimum tradeoff depends in part on the actual vertical structure in water vapor in a given profile.

[19] Figure 4 summarizes the water vapor results for the ensemble of 35 J31 vertical profiles shown in Figures 2 and 3. AATS-14 and Vaisala CWV profile means and ranges are overplotted in Figure 4a together with the number of observations at each altitude. Bias (mean) and RMS absolute Vaisala-minus-AATS CWV differences are plotted in

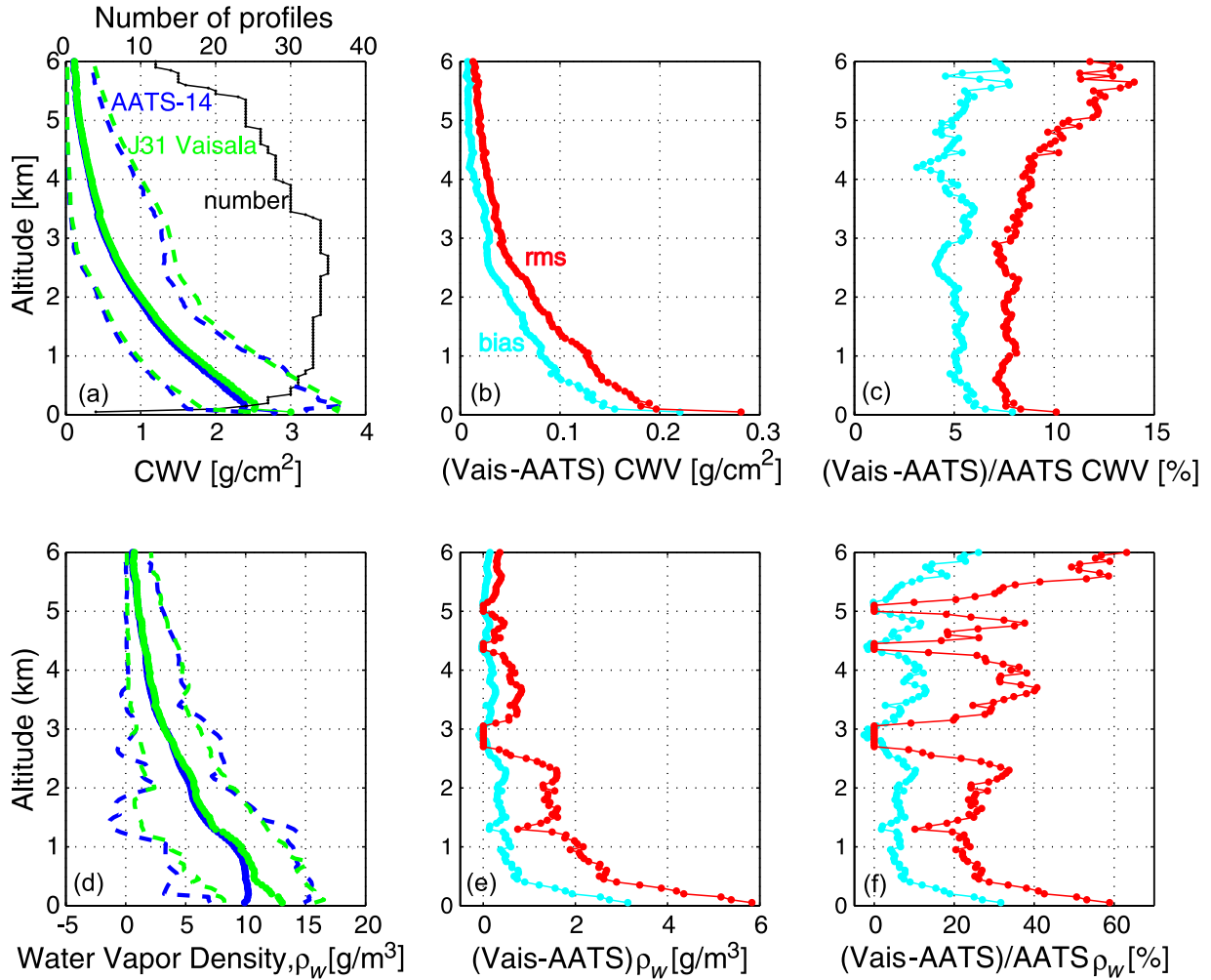


Figure 4. AATS-14 and J31 Vaisala CWV and water vapor density profile statistics: (a) CWV means (colored circles with thin lines) and ranges (colored dashed lines) and number of profiles (small black dots with line) at each altitude, (b) absolute Vaisala-minus-AATS CWV biases and RMS differences, (c) relative Vaisala-minus-AATS CWV biases and RMS differences, and (d–f) results analogous to those presented in Figures 4a–4c but for water vapor density.

Figure 4b, and relative bias and RMS CWV differences are shown in Figure 4c. Analogous plots for ρ_w are presented in Figures 4d and 4e. These data were generated by interpolating results for each profile to 50-m altitude levels between 50 m and 6.0 km ASL, with no extrapolation. Maximum mean CWV values are ~ 2.8 – 3.0 g/cm² at 50 m ASL; values decrease to 1.0 g/cm² at 2 km and ~ 0.1 g/cm² at 6 km. As shown in Figure 4c and consistent with the individual profiles presented in Figure 2, Vaisala CWV values exhibit a wet bias of $\sim 5\%$ relative to AATS CWV at most altitudes between ~ 0.7 km and 5.5 km. Biases below 0.7 km increase with decreasing altitude to a maximum of $\sim 7.5\%$ at 50 m, where only 4 profiles included measurements. Corresponding CWV RMS differences are ~ 7 – 8% below 3 km (excluding the 50-m data point), and increase to a maximum of ~ 12 – 14% above 5 km in tandem with the decrease in CWV with altitude. Mean ρ_w values range from a maximum of 10 g/m³ for AATS and ~ 13 g/m³ for the Vaisala at 50 m altitude, to ~ 5.0 g/m³ at 2 km, and < 0.5 g/m³ at 6 km. Vaisala-minus-AATS ρ_w biases vary

from approximately -3% to $+12\%$ at altitudes between 2.5 km and 5.5 km, range from 3% to 10% in the 0.5–2.5 km altitude range, and increase monotonically from $\sim 7\%$ at 0.5 km to a maximum of $\sim 30\%$ at 50 m ASL.

[20] Figure 5 further quantifies the comparison between the AATS-14 and J31 Vaisala water vapor retrievals. Figure 5a is a scatterplot of AATS versus J31 Vaisala calculations of layer-integrated water vapor, LWV, the amount of water vapor in the layer bounded by the bottom and top of the J31 profile, for the 35 profiles shown in Figure 2. The data are highly correlated, with an r^2 correlation coefficient of 0.97, but AATS LWV retrievals are biased dry by 0.17 g/cm² (7.1% of the mean J31 Vaisala value) relative to the Vaisala values, with an RMS difference of 0.21 g/cm² (8.8%). Figure 5b is a corresponding scatterplot of AATS versus Vaisala ρ_w at all altitudes. The values of r^2 and relative bias are equal to the corresponding values for the CWV comparison, but the relative RMS difference of 20.3% is significantly higher. If the analysis (plot not shown) is restricted to ρ_w data below 3 km (3353 data points), r^2

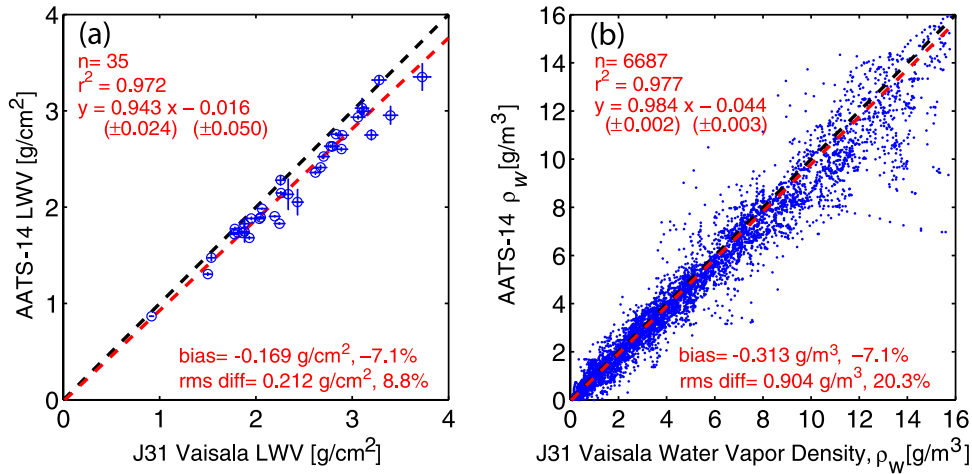


Figure 5. For the profiles shown in Figures 2 and 3, scatterplots of AATS-14 and J31 Vaisala (a) LWV and (b) ρ_w for all profile altitudes. The red dashed lines and associated fit coefficients were calculated using a weighted least squares cubic method developed by York [1966]. The black dashed lines show a 1:1 correspondence.

decreases to 0.93, but the relative bias essentially remains constant (-7.2%), and the relative RMS difference decreases to 16.8%. We note here that Schmid *et al.* [2003b] measured an AATS dry bias of 7% in ρ_w in their comparison of AATS-14 water vapor measurements with simultaneous measurements obtained by a Vaisala HMP243 and an Edge-Tech 137-C3 chilled mirror aboard the Twin Otter during ACE-Asia (Aerosol Characterization Experiment–Asia). In a more recent airborne study (at the ARM-SGP site) using AATS-14 and the EdgeTech chilled mirror aboard the Twin Otter, Schmid *et al.* [2006] report an AATS dry bias of 5% relative to the chilled mirror. During the recent ARM-SGP study AATS was equipped with the same 941-nm interference filter as that used during INTEX-ITCT 2004, but this is a different brand from that used during ACE-Asia. Schmid *et al.* [2003b] cited H₂O spectroscopy and/or the H₂O continuum used as possible sources of the AATS water vapor dry bias they found in the ACE-Asia data analysis, but we still have no definitive explanation.

[21] The error bar on each AATS LWV data point in Figure 5a represents only the uncertainty due to the effect of estimated water vapor horizontal inhomogeneity and/or temporal atmospheric variability between the top and the bottom of the J31 vertical profile. This assumes that all other sources of uncertainty (calibration, transmittance parameterization, including spectroscopic parameters, AOD) cancel. For calibration errors this is justified because the AATS LWV is calculated by subtracting the CWV measured at the top from that measured at the bottom of the profile. However, this subtraction would not correct any dry biases caused by spectroscopy or H₂O continuum. Following an approach analogous to that employed by Redemann *et al.* [2003] to calculate the uncertainty in layer AOD due to a horizontal aerosol gradient, we define the uncertainty in LWV due to a horizontal CWV gradient as

$$\delta_g LWV = \pm g \Delta x \overline{CWV}, \quad (7)$$

where \overline{CWV} is the mean columnar water vapor calculated in the layer; Δx is the horizontal distance traversed by the aircraft during the profile; and g is the relative horizontal gradient, which we compute as the ratio of standard deviation and mean of CWV during a low-level flight leg divided by the length of that leg in km. The relative horizontal gradient applied to a particular profile was that calculated from AATS measurements acquired during a low-level flight leg with $\Delta x \geq 15$ km immediately before or after the profile. For profiles for which no low-level leg was available, the mean g (0.001/km) for all low-level legs was used. The error bars on the Vaisala LWV data points were calculated from the Vaisala ρ_w uncertainties by taking the mean of the sum of $\delta\rho_w(z)$ and the RMS $\delta\rho_w$ in the profile. The latter (RMS) assumes the $\delta\rho_w(z)$ are independent and random and it may underestimate the true uncertainty; the former (sum) makes no such assumption and thus gives an upper bound on the true uncertainty. The linear fits shown in Figure 5 were calculated using the least squares cubic method developed by York [1966]. This method weights the data points in both X and Y by their respective uncertainties, and is so named because it requires the solution of a cubic equation to find the slope of the regression.

[22] In Figure 6, we compare AATS and J31 Vaisala LWV with Ronald H. Brown sonde LWV obtained by integrating the sounding data over the altitude range defined by the J31 profile. Figure 6a (AATS versus sonde) and Figure 6b (J31 Vaisala versus sonde) show results for all ship soundings (46, including 4 radiosonde/ozonesondes) within 3 hours of the 35 J31 profiles, with no screening by distance from the plane to the sounding. Corresponding r^2 values are 0.56 and 0.58, with RMS differences of ~ 0.42 g/cm², or $\sim 18\%$ of the sonde value. Agreement improves markedly if only ship soundings within 1 hour and 130 km of the J31 profile are included in the comparisons. These results are shown in Figures 6c and 6d, with r^2 values of 0.90 and 0.92, and RMS differences of 0.26 g/cm² (10.7%) and 0.20 g/cm² (8.4%), respectively, indicating

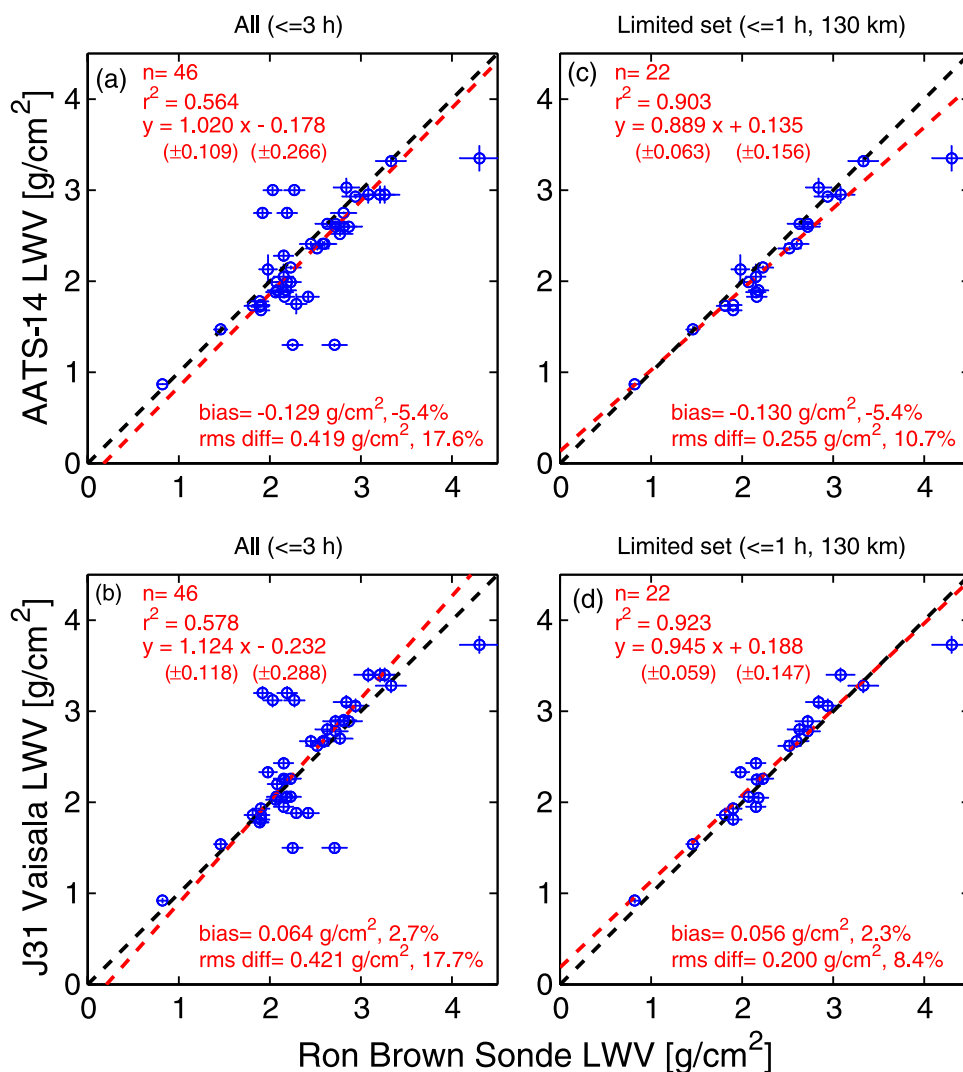


Figure 6. Comparison of LWV measured by AATS-14 and J31 Vaisala with *Ronald H. Brown* radiosonde LWV for (a and b) all soundings within 3 hours of a J31 profile, and (c and d) only soundings within 1 hour and 130 km of a J31 profile. Vertical bars show AATS LWV uncertainties; horizontal bars represent a hypothetical 5% uncertainty in sonde LWV. Black dashed lines show 1:1 correspondence. Red dashed lines are linear least squares bisectors.

the importance of collocation or the need for an independent assessment of spatial variability for the interpretation of satellite and suborbital data. AATS LWV values are biased 5.4% lower than sonde values, and J31 Vaisala values are 2.3% higher. In Figure 6, the vertical bars reflect the calculated uncertainties in AATS or Vaisala LWV, but the horizontal bars only represent a hypothetical 5% uncertainty in radiosonde LWV. Because AATS and sonde-derived LWV are both derived from measurements and are subject to measurement and retrieval uncertainties, we have used the Model II least squares bisector method [Sprenst and Dolby, 1980] to determine the regression line, which is calculated as the bisector of the minor angle between the two Model I regressions: Y on X and X on Y. In contrast to the weighted least squares regression lines shown in Figure 5 for AATS and J31 Vaisala water vapor calculations, the least squares bisector is an unweighted fit, which

is justified because the true uncertainties in sonde LWV are themselves unknown (see section 2.3).

3.2. MODIS-AATS Water Vapor Comparisons

[23] Coincident AATS-14 CWV retrievals were obtained over the ocean at aircraft altitudes below 120 m and within one hour of satellite overpass for five MODIS-Terra and five MODIS-Aqua overpasses for which MODIS IR retrievals of water vapor profiles have been derived. There were 205 MODIS IR retrieval grid cells (nominally 5 × 5 1-km pixels per cell at nadir) that contained low-altitude J31/AATS flight segments (for Terra: 126 cells on 17, 20, 22, and 29 July and 2 August; for Aqua: 79 cells on 12, 16, 21, and 23 July and 8 August). Because the MODIS TPW product is for the full atmospheric column and all AATS measurements were obtained at altitudes above the sea surface, for each MODIS grid cell containing coincident AATS retrievals we have integrated the MODIS 101-level

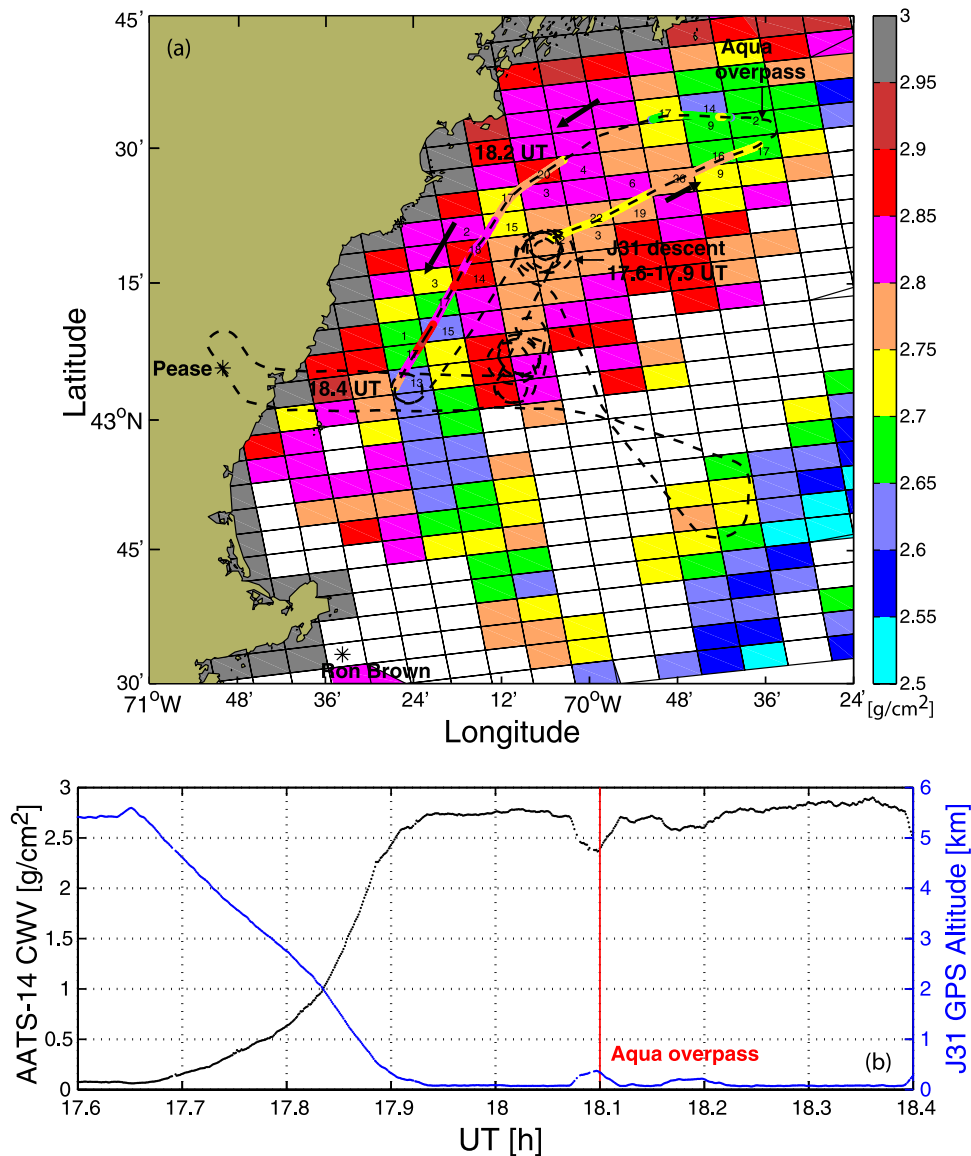


Figure 7. (a) Map showing J31 flight track (black thin dashed line) overlain on MODIS grid cells of color-coded MODIS IR TPW for Aqua overpass at 1806 UT (18.1 UT) on 21 July 2004. The J31 flight track for the low-altitude transect during the period 1754–1824 UT (17.9–18.4 UT) has been color-coded by AATS-14 CWV. (b) AATS-14 CWV and J31 altitude for the time period 1736–1824 UT (17.6–18.4 UT).

profile of water vapor mixing ratio above the altitude of the J31 for direct comparison to AATS CWV. In practice, this integral was performed over pressure (with linear interpolation between MODIS atmospheric pressure levels, as necessary) for all altitudes above the level corresponding to the mean atmospheric pressure measured on the J31 for all AATS CWV retrievals within the particular MODIS grid cell. In section 3.2.1, we illustrate our approach to comparing MODIS and AATS water vapor retrievals by examining in detail results for the Aqua overpass on 21 July 2004. We also focus on this case in section 3.3 when we introduce our approach to AATS-AIRS analysis. In section 3.2.2, we summarize the MODIS-AATS retrieval comparisons in terms of scatterplots.

[24] No screening based on the MODIS quality assurance flags has been applied to the MODIS retrievals used in our

analysis. All retrievals have been tagged as useful by the MODIS IR quality assurance flag for TPW, but according to the most recent MODIS Atmosphere QA plan [Hubanks, 2005], this flag is not reliable in regions designated not useful/bad and results in not useful pixels being incorrectly tagged as useful about 50% of the time. Regarding the MODIS cloud mask, Seemann *et al.* [2003] note that the MODIS retrieval algorithm requires that at least 5 of the 25 pixels in a 5×5 field-of-view area have a 95% or greater confidence of clear by the cloud mask and the retrieval uses the average radiance of only those pixels flagged as clear. In this paper, 188 of 205 cells included at least 20 pixels flagged as clear. Only 3 of the remaining 17 cells included fewer than 11 clear pixels, and in none of the 17 cells did the retrieved TPW value differ markedly from the values in the adjacent cells.

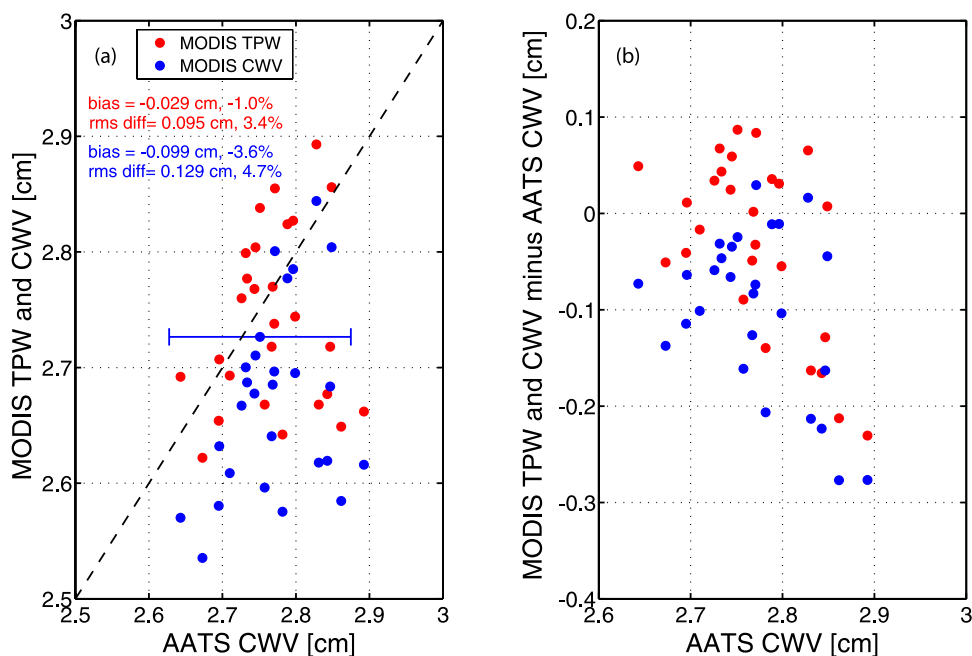


Figure 8. Comparison of MODIS and AATS-14 water vapor retrievals for MODIS data obtained during the Aqua overpass at 1806 UT on 21 July 2004 and AATS-14 data acquired during the J31 low-altitude transect during the period 1754–1824 UT: (a) MODIS TPW and CWV versus AATS CWV and (b) MODIS TPW minus AATS CWV and MODIS CWV minus AATS CWV versus AATS CWV. The horizontal bar in Figure 8a gives the representative uncertainty in AATS-14 CWV. The dashed black line represents a 1:1 correspondence.

3.2.1. MODIS and AATS Retrievals for the 21 July Aqua Overpass

[25] Figure 7a presents a map view of the J31 flight track superimposed on the MODIS IR grid cells for the MODIS-Aqua overpass at 1806 UT on 21 July. The J31 track for the entire flight is shown as a thin dashed black line. For those flight segments during the time period 1754–1824 UT (17.9–18.4 UT) when the J31 flew at or below 120 m GPS altitude, the amount of CWV measured by AATS along the track is color-coded in increments of 0.05 g/cm^2 ($= 0.05 \text{ cm}$). MODIS grid cells are color-coded using the same color scheme for the MODIS retrievals of TPW. There are 27 MODIS grid cells that contain AATS low-altitude retrievals; the number of AATS retrievals within each of these cells is printed at the center of the cell. The J31 descent during the period 1739–1756 UT (17.65–17.93 UT) (just before the low-altitude segment) is annotated, and the location of the *Ronald H. Brown* at 42.56°N , 70.56°W is also shown. Figure 7b overplots time (i.e., along track) traces of aircraft altitude and AATS-retrieved CWV for the 1736–1824 UT (17.6–18.4 UT) period. AATS CWV retrievals after the J31 descent ranged from 2.4 to 2.85 g/cm^2 , but values obtained at altitudes at or below 120 m were $\geq 2.65 \text{ g/cm}^2$. At the actual time of satellite overpass, the J31 had climbed above 120 m altitude in order to safely execute a turn from a NE heading to a WNW heading. This is also reflected in Figure 7a by the gap in AATS CWV color coding along the flight track at that time.

[26] In Figure 8, we compare MODIS retrievals of TPW and CWV with mean AATS CWV retrievals within each of the 27 MODIS grid cells for the 21 July Aqua overflight. A representative uncertainty in AATS CWV is also shown.

Since there is no published comparable MODIS uncertainty for TPW yet, none is shown. Figures 8a and 8b show that MODIS CWV underestimates AATS CWV in 25 of the 27 grid cells. For the ensemble, MODIS CWV is biased dry relative to AATS CWV by about 0.10 g/cm^2 (3.6%), with an RMS difference of 0.13 g/cm^2 (4.7%). We compare these bias and RMS differences with those reported by *Seemann et al.* [2006], who compared MODIS MOD07 over-land TPW retrievals with microwave radiometer (MWR) TPW measured at the ARM SGP site for clear sky cases between April 2001 and August 2005. In particular, for 302 MODIS-Aqua cases with no stratification by the amount of TPW, they report an average MWR-minus-MODIS bias of 0.07 g/cm^2 and an RMS difference of 0.32 g/cm^2 . For 82 Aqua “wet” ($\text{TPW} \geq 0.15 \text{ g/cm}^2$) cases, they cite corresponding bias and RMS differences of 0.34 g/cm^2 and 0.49 g/cm^2 , respectively. Hence our 21 July 2004 over-ocean case study yields absolute bias and RMS differences that are a factor of three better than the *Seemann et al.* [2006] over-land SGP Aqua “wet” results.

[27] For the 21 July case, we have also compared CWV measurements derived from a radiosonde that was launched from the NOAA R/V *Ronald H. Brown* at 1700 UT with the corresponding AATS and J31 Vaisala data acquired during the J31 1739–1756 UT descent that preceded the low-altitude transect. The mean distance between the radiosonde and the location of the J31 during its descent was 83.5 km. We do not show these results, but the three sets of CWV profile measurements agree well, with J31 Vaisala/AATS and sonde/AATS r^2 values near 1.00 and RMS differences of 0.05 g/cm^2 (6% of the mean AATS value) and 0.03 g/cm^2 (4%), respectively. LWV values in the layer traversed by the

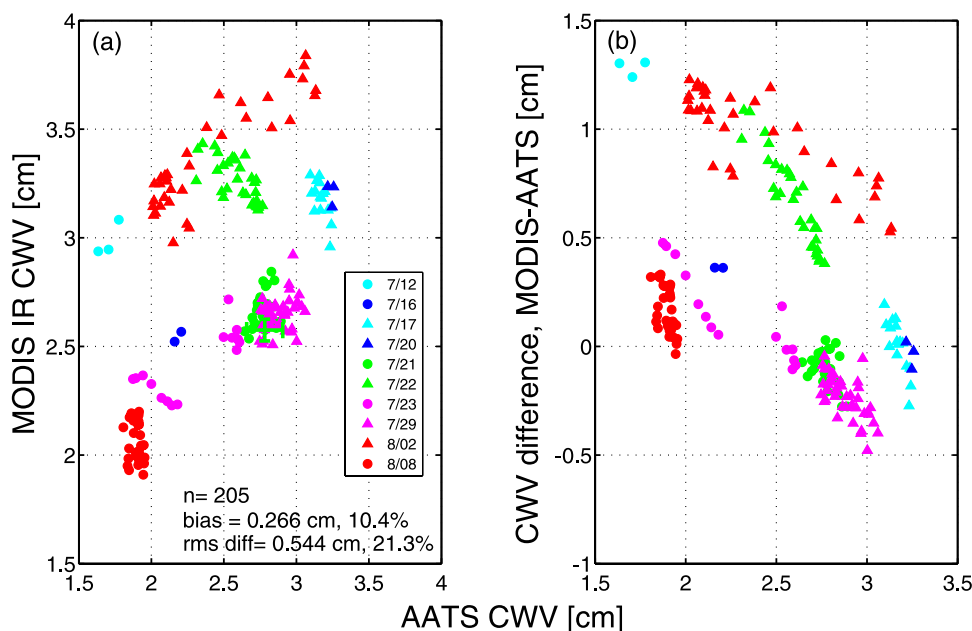


Figure 9. Comparison of MODIS IR and AATS CWV (a) retrievals and (b) differences for 205 MODIS grid cells during 5 MODIS-Aqua (solid circles) and 5 MODIS-Terra (solid triangles) overpasses. Black dashed line represents a 1:1 correspondence.

J31 during its descent (5.588–0.125 km) were 2.63, 2.78, and 2.72 g/cm^2 for AATS, J31 Vaisala, and *Ronald H. Brown* sonde, respectively. Corresponding CWV values measured or derived from measurements obtained by the three sensors at the minimum altitude of the J31 profile were 2.69, 2.84, and 2.79 g/cm^2 , respectively. The amount of water vapor measured by the sonde in the layer between the lowest altitude (0.011 km) sampled by the sonde and the bottom of the J31 profile at 0.125 km was 0.174 g/cm^2 , which yields a vertical water vapor gradient of approximately $-0.15 \text{ g}/\text{cm}^2$ per 100 m. One could use this vertical gradient to increase each of the AATS CWV measurements by the amount of water vapor below the aircraft for direct comparison with MODIS TPW. This would result in increases from 2% to 6% of the retrieved AATS CWV values. Although we have opted in favor of the more direct approach of integrating each of the 27 MODIS profiles to calculate MODIS CWV above the mean pressure (altitude) of the J31 (and, in fact, temporally and spatially near-coincident radiosonde measurements were not available for most J31/satellite comparisons), it is interesting to note that the sonde vertical water vapor gradient ($-0.15 \text{ g}/\text{cm}^2$ per 100 m) below the J31 exceeded the corresponding mean vertical gradient ($-0.09 \pm 0.02 \text{ g}/\text{cm}^2$ per 100 m) obtained from the MODIS profiles by $\sim 70\%$.

3.2.2. Ensemble Results

[28] Figure 9 presents scatterplots of MODIS CWV and MODIS-minus-AATS CWV versus AATS CWV for all 205 grid cells containing AATS retrievals during the 10 satellite overpasses. In contrast to the 21 July case for which MODIS CWV exhibited a dry bias relative to AATS CWV, for the ensemble MODIS CWV shows a wet bias of 0.27 g/cm^2 (10% of the AATS CWV); the RMS difference is 0.54 g/cm^2 (21%). The MODIS CWV retrievals appear to be stratified into two separate groups: those for the 12 July (Aqua), 22 July (Terra), and 2 August (Terra)

overflights, and those for the other 7 satellite overpasses. MODIS retrievals in all grid cells for the 12 July, 22 July and 2 August overpasses significantly overestimate the AATS values by 0.4–1.3 g/cm^2 ($\sim 15\text{--}70\%$), whereas MODIS-minus-AATS absolute differences for the other 7 cases range from -0.5 to $+0.5 \text{ g}/\text{cm}^2$. Omitting the 3 cases in the ensemble comparison would yield a bias of $-0.03 \text{ g}/\text{cm}^2$ (-1.3%) and an RMS difference of 0.20 g/cm^2 (7.8%), but there is no justification for excluding these cases. We have no explanation for this behavior at this time, but we are continuing to investigate it, as it may indicate a problem with the current version of the MODIS retrieval algorithm.

[29] In Figure 10, we stratify the data by satellite, with MODIS-Aqua results shown in Figures 10a and 10b and MODIS-Terra results presented in Figures 10c and 10d. In light of the discussion above, the results are not surprising. MODIS-Aqua retrievals agree with AATS CWV retrievals better than MODIS-Terra retrievals. In particular, MODIS-Aqua retrievals are biased high by 0.12 g/cm^2 (5.1%), with an RMS difference of 0.31 g/cm^2 (13.7%). As noted above and apparent in Figure 10, MODIS CWV significantly overestimates AATS CWV in each of the three grid cells for the 12 July case. Excluding these values would decrease the bias and RMS differences, but again there is no justification for doing so. For the ensemble of 126 grid cells for the 5 Terra overpasses, MODIS CWV retrievals exhibit a wet bias of 0.36 g/cm^2 (13.2%) and an RMS difference of 0.65 g/cm^2 (23.8%). However, as we also noted above, MODIS-Terra CWV retrievals on 22 July and 2 August are 0.4 to 1.3 g/cm^2 wetter than the corresponding AATS CWV values. Analysis of these two cases alone yields bias and RMS differences of 0.83 g/cm^2 (33.4%) and 0.87 g/cm^2 (35.0%), respectively, whereas restricting the analysis to the 17, 20, and 29 July MODIS-Terra cases yields a small dry bias of $-0.16 \text{ g}/\text{cm}^2$ (-5.4%) and an

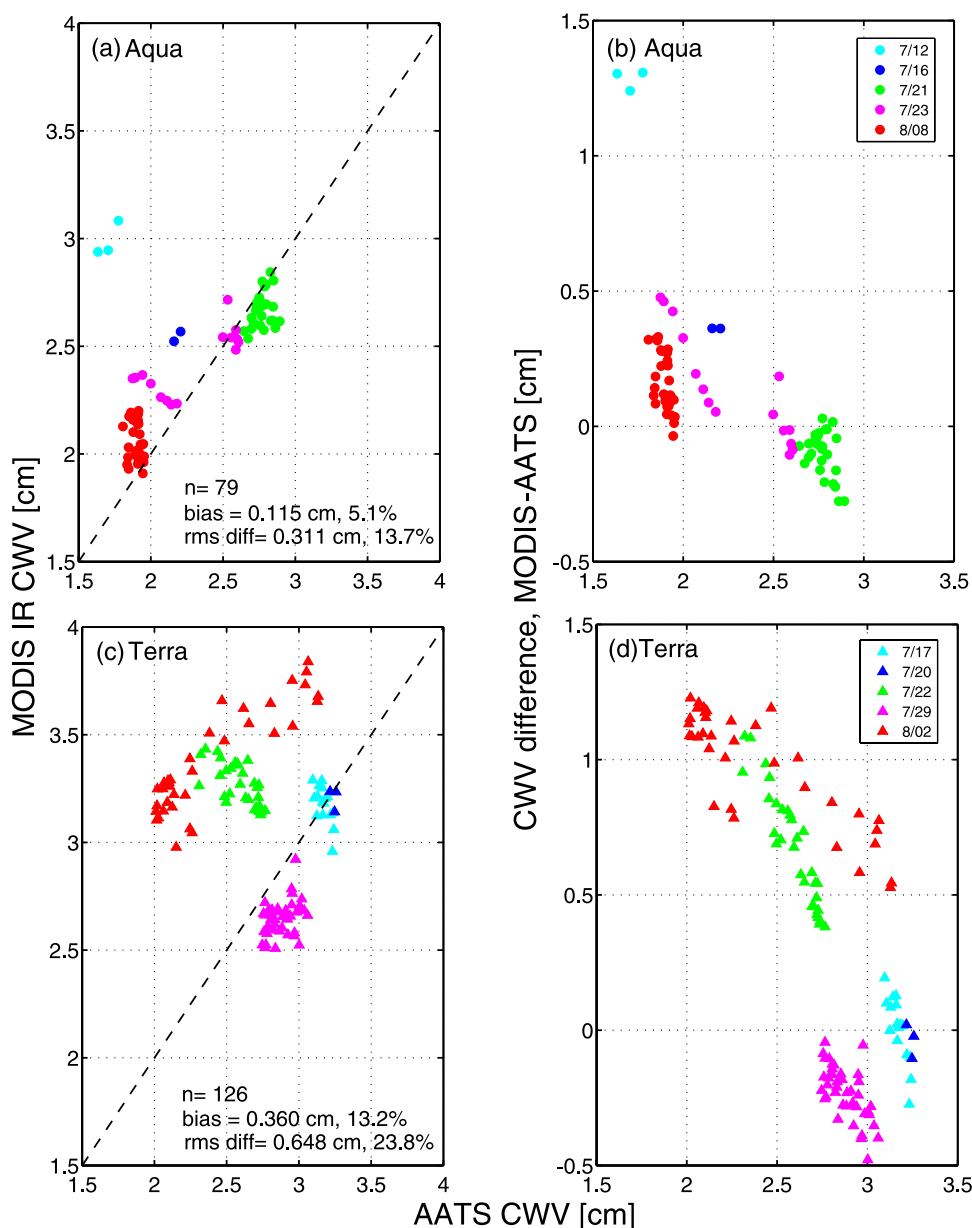


Figure 10. Same as Figure 9 but (a and b) for MODIS-Aqua comparisons only and (c and d) for MODIS-Terra comparisons only.

RMS difference of 0.22 g/cm^2 (7.3%). We note that, for 112 Terra over-land “wet” cases at the SGP site, *Seemann et al.* [2006] found that MODIS TPW retrievals exhibited a dry bias of 0.11 g/cm^2 , with a corresponding RMS difference of 0.32 g/cm^2 , compared to MWR measurements.

3.3. AIRS and J31 Sensor Water Vapor Comparisons

[30] The high spectral resolution of AIRS yields retrievals that contain much more information on the vertical distribution of water vapor than is possible from MODIS measurements, which have the horizontal resolution to better identify horizontal variability in total columnar water vapor. During ITCT, J31 ascents and/or descents near the time of the Aqua satellite overpass afforded the unique opportunity to compare coincident airborne remote (AATS-14) and in situ (Vaisala HMP243) measurements with AIRS over-ocean water vapor profile retrievals. Previously,

Gettelman et al. [2004] presented results from comparisons of AIRS oceanic water vapor retrievals and aircraft in situ water vapor measurements acquired in the upper troposphere and lower stratosphere. Other studies that have addressed or at least included validation of AIRS over-ocean water vapor retrievals have included only radiosonde measurements [*Tobin et al.*, 2006; *Fetzer et al.*, 2003], or a combination of sonde, other satellite sensor measurements, and/or numerical model results [*Fetzer et al.*, 2006; *Divakarla et al.*, 2006]. To our knowledge, ours is the first study that uses temporally and spatially coincident or near-coincident aircraft in situ and remote sensor measurements to validate AIRS over-ocean water vapor retrievals in the lower troposphere. We have identified eight Aqua overpasses for which AATS water vapor retrievals are available during near-coincident J31 vertical profiles. There were 14 separate J31 profiles flown within 90 min of these eight

Aqua overpasses, including 11 within one hour of the overpass time. In particular, these were: 1 profile each on 12, 15 and 31 July, and on 8 August; 2 profiles each on 23 and 29 July; and 3 profiles each on 16 and 21 July. In this section, we compare AIRS retrievals with AATS and J31 Vaisala water vapor retrievals derived from measurements obtained during these 14 aircraft profiles.

[31] As noted in section 2.5, we use only AIRS data extracted from the AIRS high vertical resolution (100 pressure levels) Version 4.0 L2 Support Atmospheric/Surface Product files. Although the 100-level profiles actually overresolve the vertical structure, they are particularly useful for calculating integral quantities (as done here) or in radiative transfer calculations (for which they were designed). Specifically, these files include the retrieved layer water vapor (molecules/cm²) within the layers bounded by adjacent pressure levels. These values are stored in a three-dimensional variable (100, 30, 45), where the first dimension specifies the pressure level, the second specifies subsatellite location along the satellite track, and the third specifies the across-track location. AIRS retrievals are available at 31 pressure levels (each corresponding to the base of a layer) between 407.47 hPa (~maximum altitude attained during any J31 profile) and 1100 hPa. For each profile, the index of the first pressure level above the mean surface is also included in the archived data files and, because the retrievals below this surface are extrapolated, the surface value must be calculated by interpolation [Olsen *et al.*, 2005b]. The AIRS retrieval data sets include numerous control flags that provide information about the quality of the retrieved products. These are discussed in detail by Susskind *et al.* [2006]. Following Tobin *et al.* [2006] and Fetzer *et al.* [2006], we screen the AIRS retrievals by using two of the AIRS quality flags: *Qual_H2O* and *Qual_Temp_Profile_Bot*. These can have values of 0, 1, or 2 corresponding to retrievals of highest, good, and poor (unacceptable) quality, respectively. *Qual_H2O* is the overall quality flag for water vapor and equals zero if the microwave-only part of the retrieval algorithm converged. *Qual_Temp_Profile_Bot* indicates temperature convergence in the lowest 2–3 km of the profile (700 hPa and below), but it equals zero only if the IR temperature profile retrieval algorithm converged throughout the profile. As noted by Fetzer *et al.* [2006], since the temperature solution from the IR observations must converge for the water vapor solutions to proceed, retrievals with *Qual_Temp_Profile_Bot* = 0 have the highest information content.

[32] We compare AIRS water vapor retrievals with AATS and Vaisala water vapor measurements by examining differences for (1) the layer defined by the bottom and top of J31 profiles (section 3.3.2) and (2) the individual layers defined by the AIRS retrieval pressure levels (section 3.3.3). To set the stage for these comparisons, we first show (section 3.3.1) retrievals for the same case: the 21 July Aqua overpass at 1806 UT and the coincident J31 descent during the period 1736–1754 UT, discussed in section 3.2.1.

3.3.1. AIRS and J31 Sensor Retrievals for the 21 July Aqua Overpass

[33] Figure 11a presents a map view of the J31 flight track (color-coded by aircraft altitude) on 21 July and the center point locations of the 20 AIRS profiles retrieved within 150 km of the J31 profile. In addition to the 1736–

1754 UT spiral descent from 5.6 km to 0.125 km, the J31 flight pattern on this day also included a ramped ascent from 1706 to 1724 UT (17.1 to 17.4 UT) after takeoff from Pease, and another spiral descent from 1854 to 1906 UT (18.9 to 19.1 UT). Figure 11b overplots the CWV profiles measured by AATS and by the J31 Vaisala during the J31 descent with the AIRS CWV profiles retrieved within the AMSU footprints centered at the locations shown in Figure 11a. (Recall that although each AMSU footprint encompasses nine AIRS footprints, only one AIRS water vapor retrieval at the coarser AMSU resolution is archived for each AMSU footprint.) The AIRS retrievals use the same symbol and color scheme shown in Figure 11a, and the legend also includes the across-track (first, e.g., 25) index and along-track (second, e.g., 9) index corresponding to the indices listed next to each AIRS center location shown in Figure 11a. The vertical coordinate in Figure 11b and in subsequent plots showing AIRS data is atmospheric pressure, because that is the vertical coordinate included in the AIRS product files and it is routinely measured on the J31. The AIRS CWV at each altitude has been calculated by summing all AIRS layer water vapor values at and above that altitude. The AIRS data points at the largest pressure (lowest altitude) for each retrieval have been calculated using the interpolation procedure prescribed by Olsen *et al.* [2005b].

[34] For comparison with the archived AIRS water vapor retrievals within specified pressure layers, we have interpolated within the AATS and J31 Vaisala water vapor retrievals to calculate the amount of water vapor, LWV_A, within the layers defined by the AIRS pressure levels for which J31 data are available. Here we use the acronym LWV_A to distinguish from LWV, the water vapor in the layer bounded by the minimum and maximum altitudes of the J31 profile. In Figure 12, we overplot AIRS LWV_A retrievals centered at each of the 20 locations shown in Figure 11a with the AATS and J31 Vaisala LWV_A calculated from the measurements acquired during the 1736–1754 UT J31 descent. Also shown are the AIRS-minus-AATS and AIRS-minus-Vaisala LWV_A differences. The frames shown in Figure 12 are arranged from upper left to lower right in order of increasing distance from the center of the AIRS retrieval grid cell to the mean location of the J31 spiral descent from 1736 to 1754 UT. Each frame is labeled with this distance and also with the across-track and along-track indices of the AIRS retrieval center point location. On the basis of the LWV_A differences, a number of the AIRS retrieved profiles (e.g., profiles at locations [25, 10] – 92.8 km, [26, 10] – 87.4 km, [26, 11] – 36.6 km) appear to agree quite well with the AATS and Vaisala retrievals. In order to compile meaningful statistics, we have calculated LWV_A for all ITCT J31/AIRS near-coincident profile measurements. These results will be discussed in detail in section 3.3.3.

3.3.2. Layer Water Vapor (LWV) Comparisons for J31 Profile Layers

[35] As noted above, there were 8 Aqua overpasses and 14 J31 profiles for which near-coincident AIRS and J31 data are available. We have calculated LWV for AIRS profile retrievals within 150 km of each J31 profile by integrating the AIRS data over the altitude (pressure) range of the J31 profile. AATS LWV has been calculated for each J31 profile by subtracting the CWV measured at the top of the profile from that measured at the bottom, and for the J31

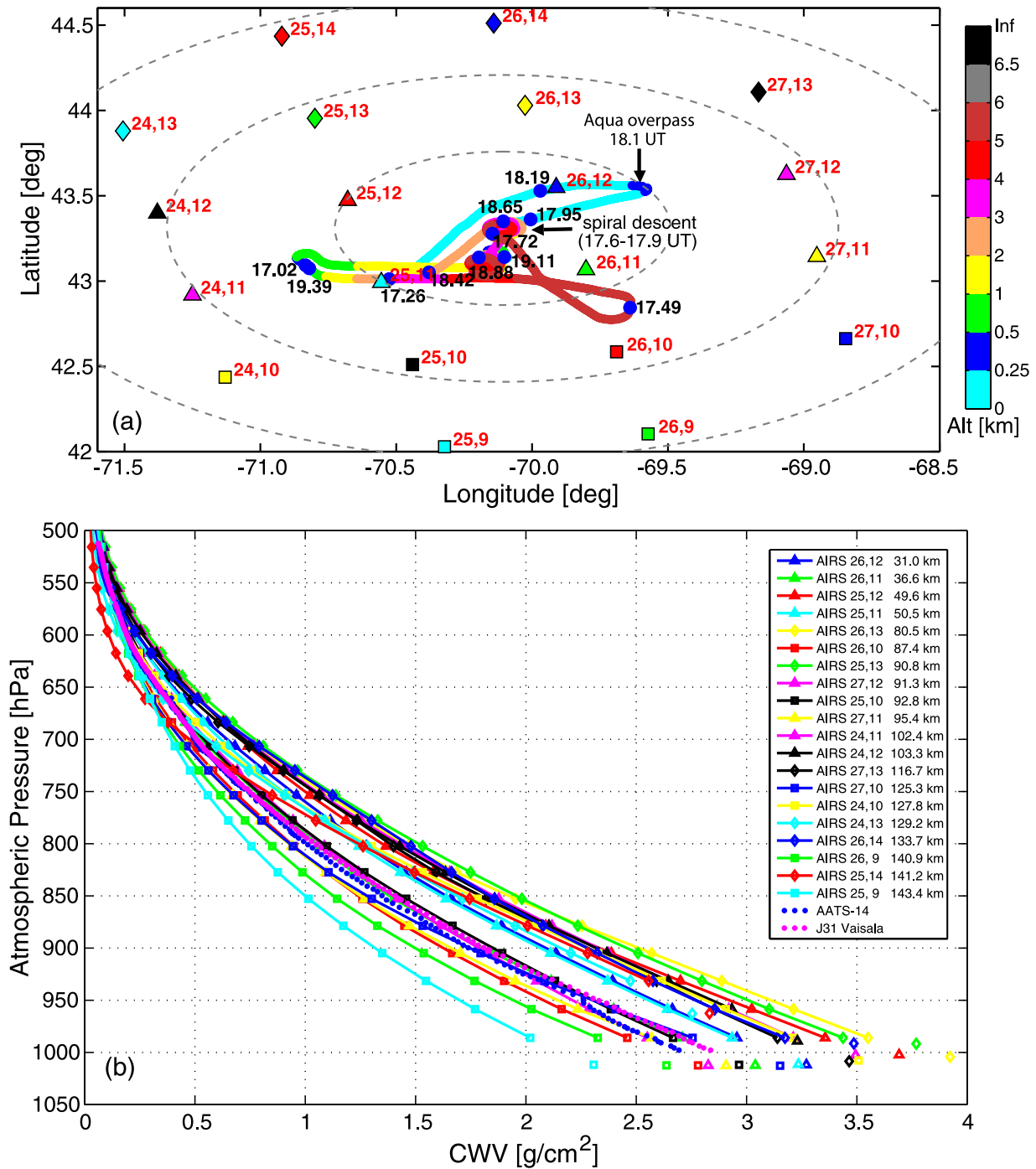


Figure 11. (a) Map view of J31 flight track (color coded by aircraft altitude) on 21 July and the center point locations of the 20 AIRS water vapor vertical profile retrievals within 150 km of the J31 1736–1754 UT (17.6–17.9 UT) spiral descent. Times (UT) corresponding to J31 locations (blue dots) are listed in black, red numbers list cross-track and along-track data indices, and dashed black ellipses delineate distance in 50-km increments from the mean location of the J31 spiral descent. (b) Profiles of AIRS CWV retrievals at each of the AIRS locations; AATS-14 and J31 Vaisala CWV measured during the J31 descent.

Vaisala by integrating its ρ_w measurements. In Figure 13, we explore the behavior of the absolute and relative AIRS-minus-AATS LWV differences as a function of the distance from the AIRS retrieval center point location to the mean location of the J31 profile. In Figure 13, all AIRS retrievals

within 150 km of the J31 for a particular J31 profile have been color-coded using the same symbol/color combination, but a different combination has been used to identify data pertaining to each J31 profile. Figure 13a shows the absolute LWV differences, and Figure 13b shows the relative differ-

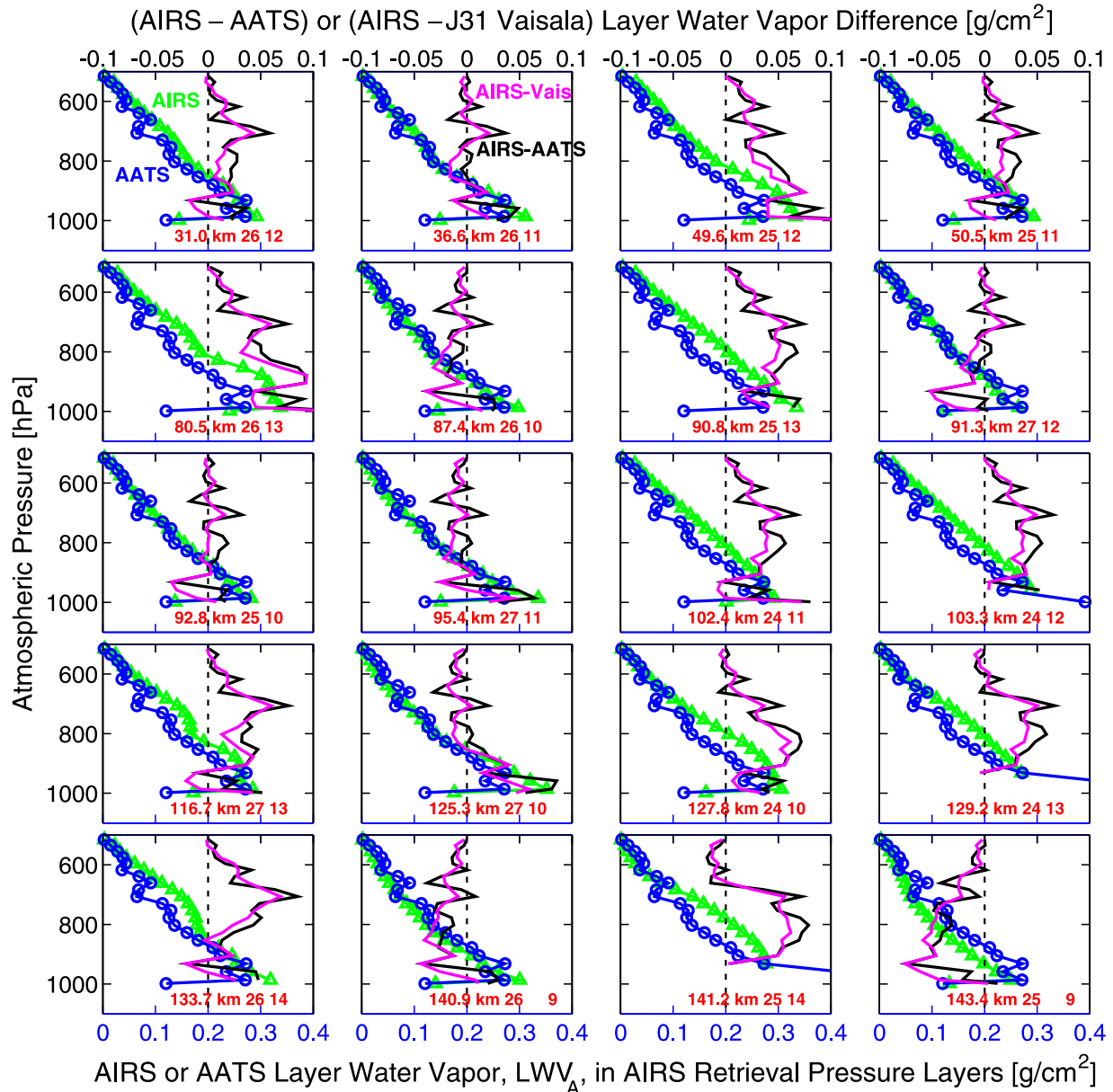


Figure 12. Profiles of AIRS (green) and AATS-14 (blue) LWV_A retrievals (bottom x axis scale), and AIRS-minus-AATS (black) and AIRS-minus-Vaisala (magenta) retrievals differences (top x axis scale) within the AIRS retrieval pressure layers for the J31 1739–1756 UT descent and the AIRS profiles shown in Figure 11. Text in each frame gives the mean distance from the J31 profile to the AIRS retrieval center point, in addition to the across-track and along-track indices of the AIRS location.

ences. For each profile, the legend lists the date, Aqua overpass time, J31 profile times, and vertical extent (in hPa) of each J31 profile. Most mean LWV differences fall between $-0.6 \text{ g}/\text{cm}^2$ ($\sim 20\%$ of the AATS value) and $+1.0 \text{ g}/\text{cm}^2$ ($\sim 50\%$ of the AATS value) for AIRS profiles within 100 km of the J31 profile.

[36] Figure 14 presents scatterplots of AIRS versus AATS LWV for those AIRS retrievals for which $\text{Qual_H}_2\text{O} = 0$. Figures 14a and 14b show results for AIRS retrievals within 150 km of a particular J31 profile for $\text{Qual_Temp_Profile_Bot} = 2$ and $\text{Qual_Temp_Profile_Bot} = 0$, respectively, and Figures 14c and 14d show analogous results for AIRS

retrievals within 80 km. Table 2 lists the statistics of the AIRS-AATS LWV comparisons, in addition to analogous statistics of AIRS-Vaisala LWV comparisons (not shown), and, for the sake of completeness, results of AATS-Vaisala LWV comparisons for the subset of 14 aircraft profiles. Examination of Figure 14 and Table 2 leads to the following observations:

[37] 1. AIRS LWV retrievals exhibit a wet bias relative to AATS-14 and J31 Vaisala measurements. AIRS retrievals agree somewhat better with the Vaisala than with the AATS-14 values, and this is consistent with the finding

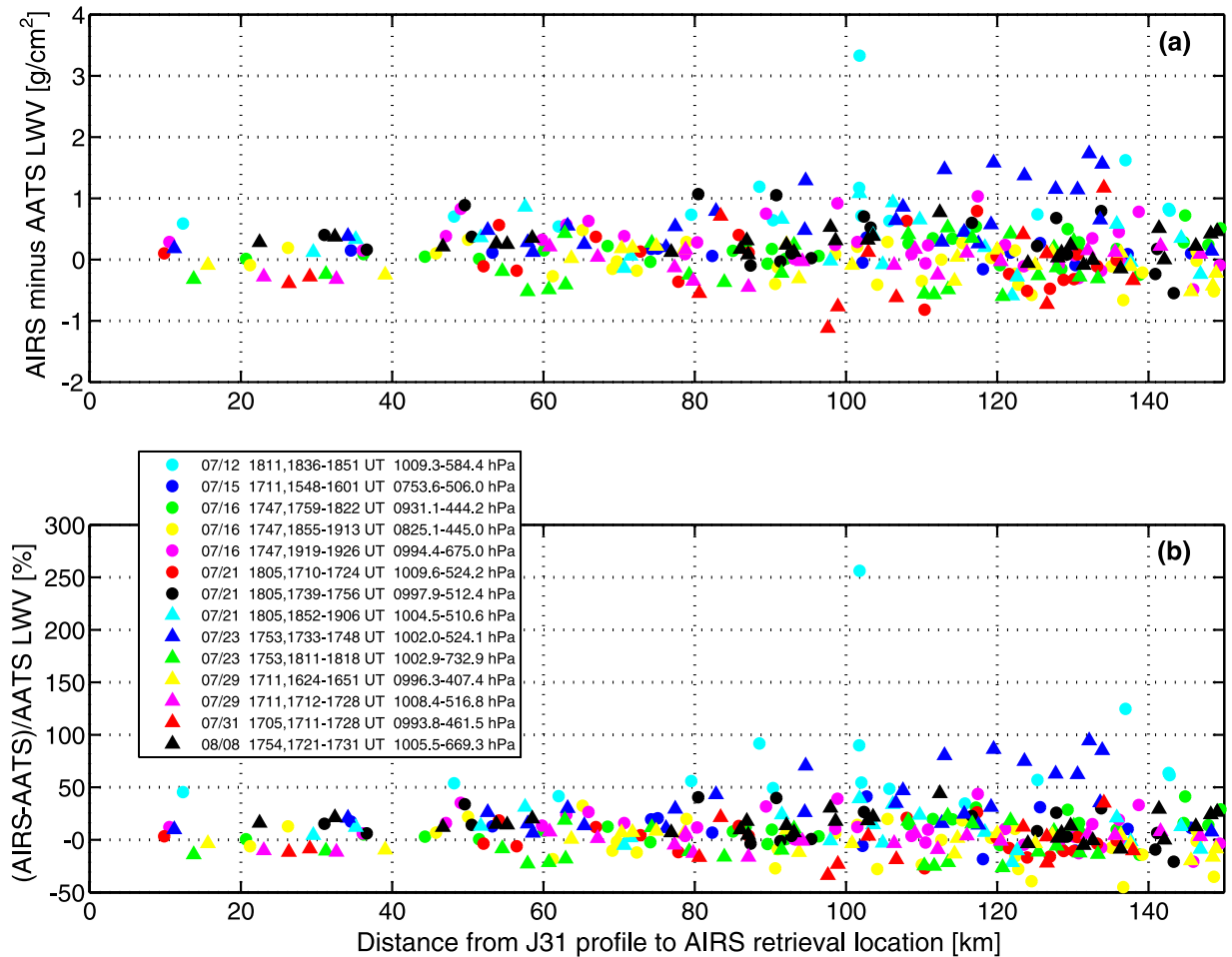


Figure 13. Dependence of AIRS-minus-AATS (a) absolute and (b) relative LWV differences on the distance from the AIRS retrieval location to the mean location of the appropriate J31 profile for 14 separate J31 profiles during 8 Aqua overpasses. Legend gives date, Aqua overpass time, J31 profile times, and vertical extent of each J31 profile.

that AATS measurements are biased 4.3% dry relative to the Vaisala measurements for the subset of 14 J31 profiles.

[38] 2. For the AIRS-AATS and the AIRS-Vaisala LWV comparisons, agreement improves if AIRS retrievals are limited to those located within 80 km of the J31 profile. For the highest information content AIRS water vapor retrievals ($Qual_Temp_Profile_Bot = 0$), bias differences decrease from 8.8% (150 km) to 5.8% (80 km) for AIRS-AATS and from 4.0% to 1.0% for AIRS-Vaisala. RMS differences decrease from 21.5% (150 km) to 16.4% (80 km) for AIRS-AATS, and 18.5% to 12.8% for AIRS-Vaisala.

[39] 3. As noted in section 3.3, AIRS retrievals with $Qual_Temp_Profile_Bot = 2$ represent poor (actually, unacceptable) retrievals. Nevertheless, our results for values of bias and RMS differences suggest that agreement between AIRS and J31 sensor LWV improves only marginally if analysis is restricted to those AIRS retrievals of highest quality.

[40] The rationale for discriminating by distance from the AIRS profile to the J31 profile and for limiting the scatterplots to all profiles within 150 km and to those within 80 km is shown in Figure 15. Figure 15 examines the variation of r^2 and of RMS differences, calculated at

10-km increments in distance, for AIRS-AATS and for AIRS-Vaisala comparisons as a function of the maximum allowable distance. Figure 15a presents results for $Qual_Temp_Profile_Bot = 2$ and shows that r^2 decreases markedly for distance thresholds between 30 and 50 km and even more dramatically beyond 80 km. For retrievals with $Qual_Temp_Profile_Bot = 0$ (Figure 15b), the largest decreases in r^2 occur between 50 and 70 km, and beyond 110 km. The RMS difference variation is essentially a mirror image of the corresponding r^2 variation. If the results for distances less than 50 km are ignored because of the relatively low number of AIRS retrievals at those distances, then a maximum distance threshold of 80 km appears to be a reasonable choice for presentation of the results.

3.3.3. Layer Water Vapor (LWV_A) Comparisons for AIRS Pressure Layers

[41] In Figures 16 and 17, we compare AIRS retrievals of layer water vapor, LWV_A, for 26 layers defined by the AIRS pressure levels between 986.07 hPa and 407.5 hPa with corresponding J31 retrievals of LWV_A calculated for the same layers. The AATS and Vaisala values were calculated by interpolation, as described above. Figure 16 shows results for the AIRS and AATS comparison for a distance

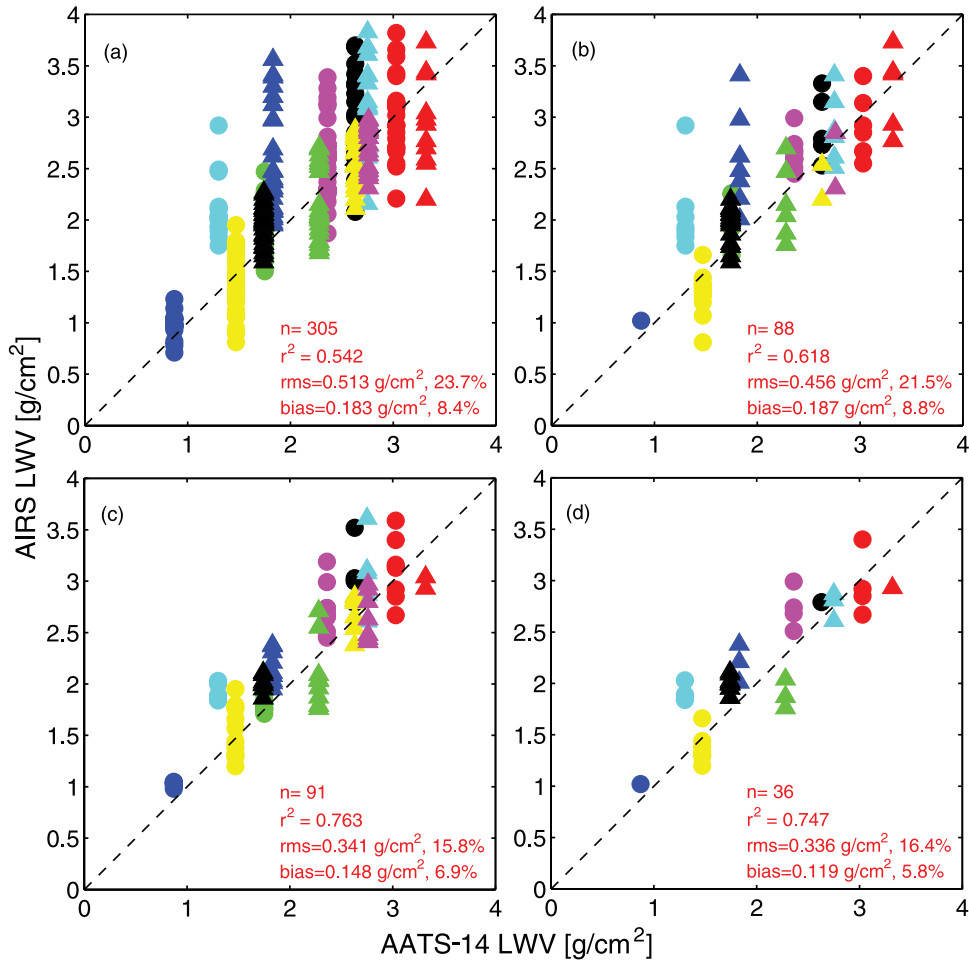


Figure 14. Scatterplot comparisons of AIRS and AATS LWV for (a) AIRS retrievals within 150 km of a J31 profile for AIRS retrieval control flag *Qual_Temp_Profile_Bot* = 2, (b) AIRS retrievals within 150 km of a J31 profile for *Qual_Temp_Profile_Bot* = 0, (c) AIRS retrievals within 80 km of a J31 profile for flag *Qual_Temp_Profile_Bot* = 2, and (d) AIRS retrievals within 80 km of a J31 profile for *Qual_Temp_Profile_Bot* = 0. Dashed lines represent the 1:1 correspondence and are shown for reference.

threshold of 150 km only. Figures 16a–16c are for *Qual_Temp_Profile_Bot* = 2 and Figures 16d–16f are for *Qual_Temp_Profile_Bot* = 0. In Figure 16a, the means and ranges of LWV_A in each pressure layer are plotted at the

bottom pressure boundary. The number of AIRS retrievals included in each pressure layer and the number of AATS data points are also shown. Figure 16b shows bias and RMS AIRS-minus-AATS LWV_A differences, and Figure 16c

Table 2. Comparison of Layer Water Vapor (LWV) Retrievals by AATS-14, J31 Vaisala, and AIRS

x	y	Maximum Distance, km	<i>Qual_Temp_Bot</i> ^a	n	r ²	RMS Difference		Bias Difference	
						g/cm ²	%	g/cm ² ^b	% ^c
J31 Vaisala	AATS-14			14	0.987	0.127	5.5	−0.099	−4.3
AATS-14	AIRS	150	2	305	0.542	0.513	23.7	0.183	8.4
AATS-14	AIRS	150	0	88	0.618	0.456	21.5	0.187	8.8
AATS-14	AIRS	80	2	91	0.763	0.341	15.8	0.148	6.9
AATS-14	AIRS	80	0	36	0.747	0.336	16.4	0.119	5.8
J31 Vaisala	AIRS	150	2	305	0.564	0.474	20.9	0.080	3.6
J31 Vaisala	AIRS	150	0	88	0.639	0.411	18.5	0.089	4.0
J31 Vaisala	AIRS	80	2	91	0.805	0.283	12.5	0.049	2.2
J31 Vaisala	AIRS	80	0	36	0.807	0.275	12.8	0.021	1.0

^a*Qual_Temp_Bot* (= *Qual_Temp_Profile_Bot*) = 0 for highest information content water vapor retrieval [Fetzer et al., 2006].

^bCalculated as mean(y − x).

^cCalculated as 100*mean(y − x)/mean(x).

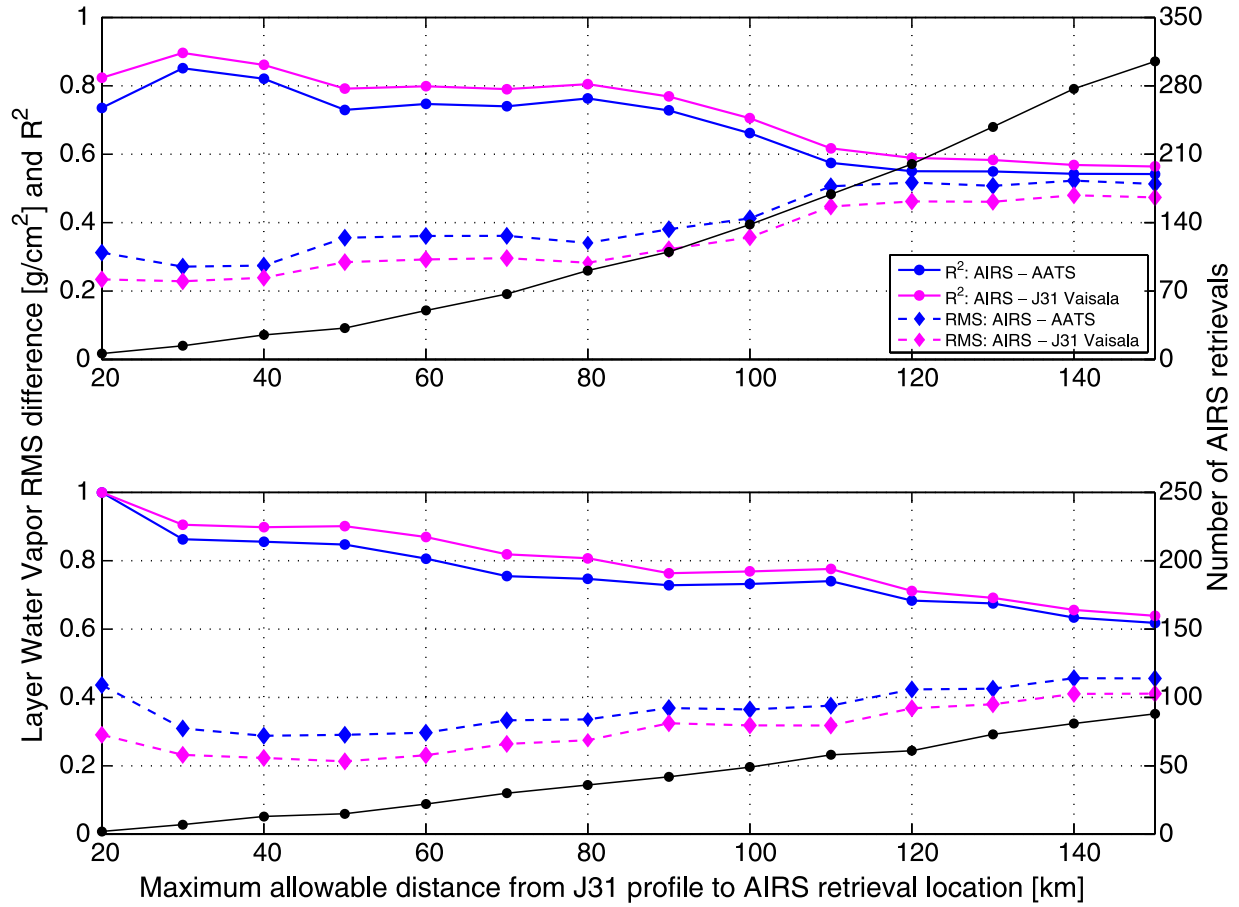


Figure 15. Variation of RMS differences (dashed) and r^2 (solid) for AIRS-AATS and AIRS-Vaisala LWV retrievals as a function of the maximum allowable distance from the J31 profile to the AIRS retrieval location for (a) *Qual_Temp_Profile_Bot* = 2 and (b) *Qual_Temp_Profile_Bot* = 0. The numbers of AIRS retrievals included in the analyses are also shown (black).

presents the relative differences. Bias and RMS percent differences have been weighted by the amount of water vapor in the layer, in keeping with the approach used by *Susskind et al.* [2003] and *Tobin et al.* [2006]. Analogous results for *Qual_Temp_Profile_Bot* = 0 are presented in Figures 16d–16f. Figure 17 presents LWV_A results for AIRS and AATS (Figures 17a–17c) and AIRS and J31 Vaisala (Figures 17d–17f) for AIRS retrievals with *Qual_Temp_Profile_Bot* = 0 and within 80 km of a J31 vertical profile.

[42] Examination of Figures 16 and 17 leads to the following observations regarding comparisons of LWV_A :

[43] 1. AATS LWV_A retrievals show more variation than do the retrievals from the in situ and the satellite sensors. This result is attributed to the nature of the basic AATS retrieval, CWV, which is dependent on the total amount of water vapor in the column above the sensor at each altitude and, hence, is more sensitive to horizontal inhomogeneities in water vapor than retrievals from the other two sensors. However, data derived from measurements by both J31 sensors are susceptible to water vapor spatiotemporal variability due to advection or spatial inhomogeneity during the aircraft profile.

[44] 2. When all AIRS profiles within 150 km of the J31 profiles are included, AIRS retrievals exhibit positive excursions from the mean that are 2–4 times the corresponding

AATS values, as evidenced by the respective range of observed retrievals (purposely truncated in Figures 16a and 16d), but AIRS negative excursions are less than those of AATS.

[45] 3. When AIRS profile retrievals within 150 km of the J31 and with *Qual_Temp_Profile_Bot* = 2 are included, AIRS mean retrievals exceed corresponding AATS means in all layers below 600 hPa, with biases ranging from ~ 0.005 to 0.025 g/cm^2 . Since these AIRS profiles are the lowest-quality AIRS retrievals, they were not expected to agree well with the AATS data. Nevertheless, relative biases are generally $<10\%$ for layers below 707 hPa (top of the layer with the base at 730 hPa). Relative biases are generally 20–30% between 700 and 600 hPa. The one exception is the large bias of $\sim 0.025 \text{ g/cm}^2$ ($\sim 55\%$) for the 684–661 hPa layer. This is attributed to spatial or temporal variability in the water vapor during one or more J31 profiles included in the mean and leads to slightly negative AATS LWV_A retrievals near 700 hPa in those few profiles and an artificially low mean value in the layer between 707 and 684 hPa. The peak in the AIRS-AATS bias in the layer with its base at 958 hPa is likely also due to atmospheric variability in the CWV above the J31 that results in an artificially low mean AATS retrieval. The AIRS-AATS comparisons exhibit large relative RMS differences above

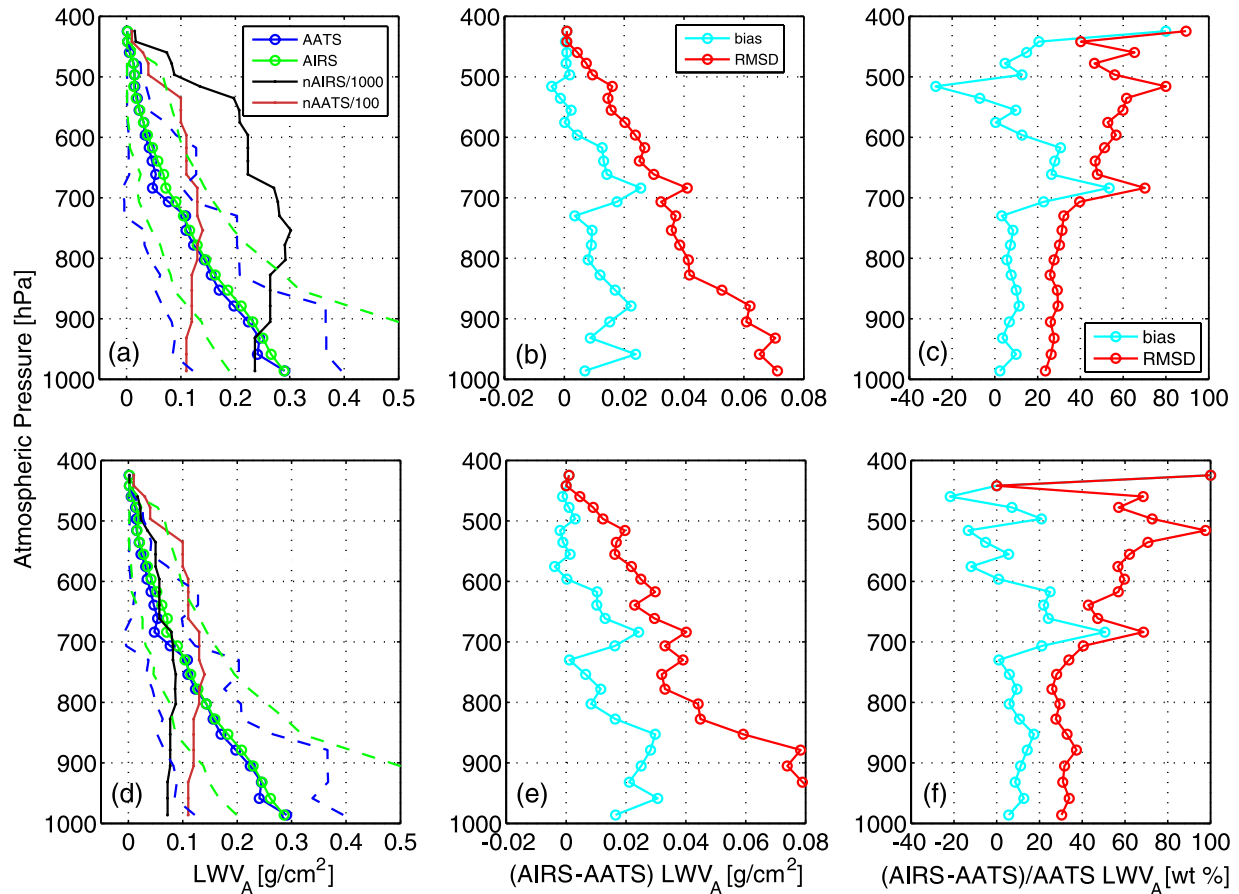


Figure 16. Comparisons of AIRS and AATS-14 LWV_A retrievals for AIRS retrievals within 150 km of a J31 vertical profile and with (a–c) $Qual_Temp_Profile_Bot = 2$ and (d–f) $Qual_Temp_Profile_Bot = 0$. Figures 16a and 16d show means (open circles with solid lines) and ranges (dashed lines) of AIRS and AATS LWV_A profile retrievals, numbers of AIRS and AATS retrievals at each altitude; Figures 16b and 16e show absolute AIRS minus AATS LWV_A biases and RMS differences; and Figures 16c and 16f show relative AIRS minus AATS LWV_A biases and RMS differences.

700 hPa due to the small mean LWV_A values at those altitudes. For the highest-quality AIRS retrievals (Figures 16e and 16f), results change only slightly. The number of AIRS retrievals included in the analysis for each layer decreases significantly (by up to 70% for the 754–730 hPa layer), but the largest change in the statistics is a small increase in the biases and RMS differences for layers below 800 hPa.

[46] 4. Restricting the analysis to AIRS profiles located within 80 km of the J31 (Figure 17) also reduces the number of AIRS retrievals in each layer (at least below 500 hPa) significantly from the number included for a distance threshold of 150 km. For AIRS LWV_A retrievals, resultant positive excursions from the mean decrease markedly, and the range of values becomes comparable to the range of the AATS and Vaisala retrievals. Bias and RMS difference curves shift to the left (or smaller values for RMS differences and for positive biases), with an increase in the number of negative bias values, especially below 750 hPa. AIRS–AATS biases vary from -2% to $+6\%$ below 729 hPa, and from -25% to $+20\%$ above 670 hPa, with corresponding RMS differences of $\sim 20\%$ below 700 hPa and 40–100% above 700 hPa. Corresponding AIRS–Vaisala

biases vary from -5% to $+5\%$ below 700 hPa, and from -35% to $+20\%$ above 700 hPa, with RMS differences of 15–20% below 700 hPa and 35–80% above 700 hPa.

[47] Our results for AIRS–J31 sensor LWV_A bias and RMS differences below 700 hPa are consistent with those reported for the 1000–700 hPa layer by Fetzer *et al.* [2004] for AIRS–radiosonde comparisons at four locations in California and Hawaii for the period December 2002 to January 2003. In particular, they found bias and standard errors of $-4.9 \pm 24\%$ and $+3.1 \pm 19\%$ for AIRS TPW retrievals of 1.1 cm at San Diego and Vandenberg, respectively; and corresponding values of $-0.3\% \pm 14\%$ and $+2.7 \pm 14\%$ for AIRS TPW retrievals of ~ 2 cm at Hilo and Lihue, respectively. Recently, Tobin *et al.* [2006] conducted an analysis of ARM site best estimates (derived by measurements from a variety of sensors including RS90 radiosondes) of temperature and water vapor for validation of AIRS retrievals. For the highest-quality AIRS retrievals, they report AIRS wet biases of $<5\%$ relative to the ARM site best estimates for water vapor retrievals in 2-km layers below 400 hPa for both the TWP (Tropical Western Pacific) and the SGP data sets. These values are very similar to our

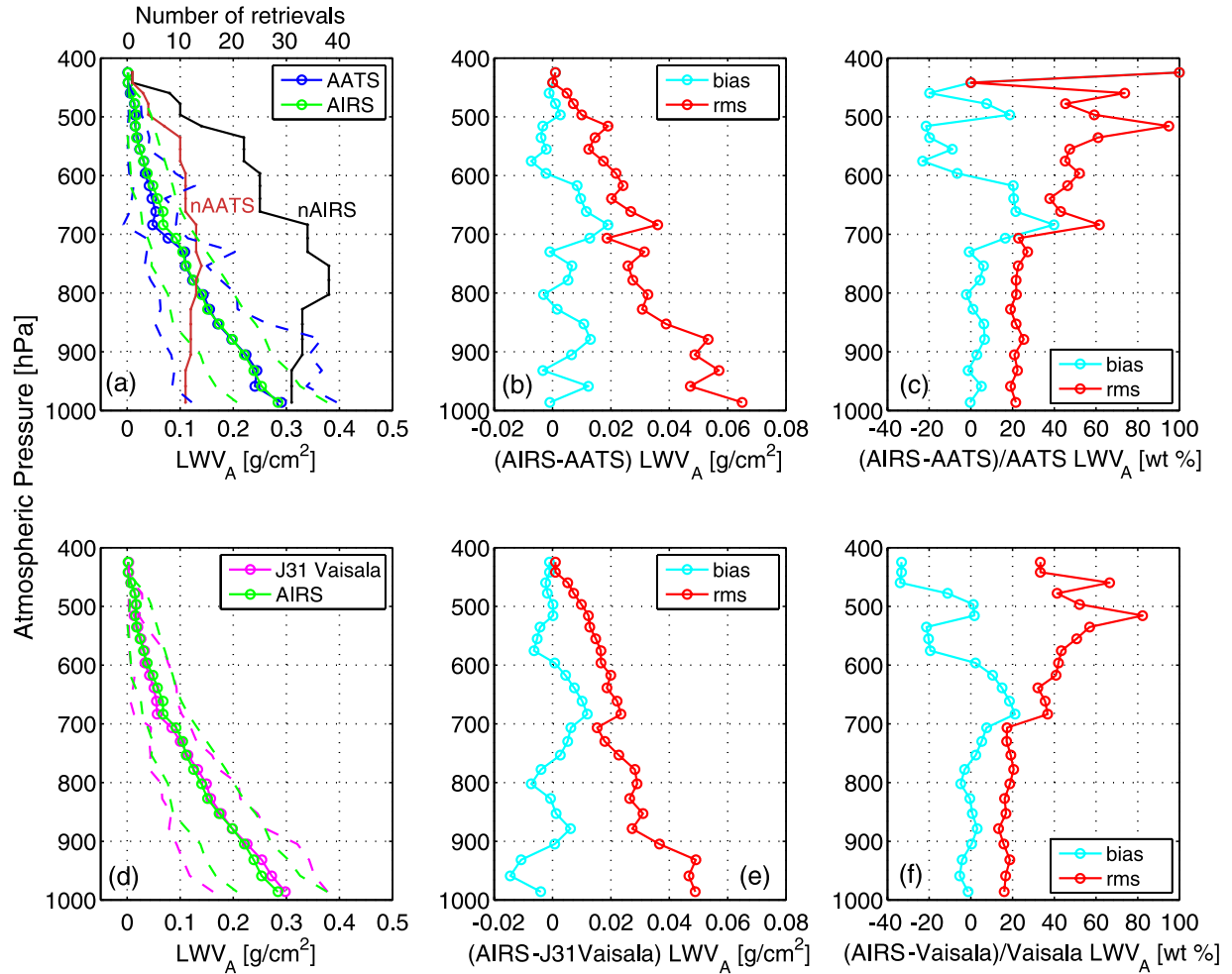


Figure 17. Comparisons of AIRS and J31 sensor LWV_A retrievals for AIRS retrievals with *Qual_Temp_Profile_Bot* = 2 and within 80 km of a J31 vertical profile. (a) Means (open circles with solid lines) and ranges (dashed lines) of AIRS and AATS LWV_A profile retrievals, numbers of AIRS and AATS retrievals at each altitude; (b) absolute AIRS-minus-AATS LWV_A biases and RMS differences; and (d–f) same as Figures 17a–17c but for AIRS–J31 Vaisala comparisons.

results below 700 hPa for the highest-quality AIRS retrievals within 80 km of the J31 profiles. In this study, we find relative RMS differences of $\sim 20\%$ below 700 hPa and $\geq 40\%$ above that altitude. *Tobin et al.* [2006] report RMS differences of $\sim 25\%$ for the SGP comparisons, but RMS differences of $\sim 10\%$ for the TWP data. In an intercomparison of AIRS retrievals with global radiosonde observations, satellite retrievals, and model forecast profiles, *Divakarla et al.* [2006] report biases for clear-only cases on the order of $\pm 5\%$ below 500 hPa, with RMS differences of 10–20% below 800 hPa and increasing to $\sim 30\%$ between 600 hPa and 500 hPa.

4. Summary and Conclusions

[48] Airborne Sun photometer measurements acquired over the Gulf of Maine during INTEX-ITCT 2004 have been analyzed to yield retrievals of columnar water vapor and profiles of water vapor density. AATS-14 measurements acquired during low-level (typically 60–120 m ASL) J31 transects designed to coincide temporally and spatially with satellite overpasses allowed comparison of AATS CWV

with MODIS over-ocean IR retrievals of CWV obtained during 5 Aqua and 5 Terra overpasses. AATS water vapor profile retrievals have been compared with simultaneous in situ measurement of water vapor density by an onboard Vaisala humidity sensor and with temporally and spatially near-coincident measurements by radiosondes released from the NOAA R/V *Ronald H. Brown*. AATS and J31 Vaisala profile measurements obtained near the time of satellite overpass have also been compared with AIRS water vapor retrievals from data obtained during 8 Aqua overpasses.

[49] Comparison of AATS-14 and J31 Vaisala retrievals of the amount of LWV during 35 aircraft vertical profiles yields an r^2 of 0.97 and an RMS difference of 0.21 g/cm^2 (8.8%). Comparison of corresponding ρ_w values calculated at 20–50 m vertical resolution for all of these profiles yields an r^2 of 0.98 and an RMS difference of 0.90 g/m^3 (20.3%). For the composite data sets, AATS retrievals of LWV and ρ_w slightly underestimate the corresponding Vaisala retrievals by amounts that increase with increasing LWV and ρ_w , with biases of -7.1% . *Schmid et al.* [2003b] and *Schmid et al.* [2006] found similar biases in AATS ρ_w compared to

measurements by another Vaisala HMP243 and by a chilled mirror. *Schmid et al.* [2003b] implied that uncertainties in the H₂O spectroscopy and/or the H₂O continuum could be sources of the AATS/in situ sensor water vapor differences and noted then that the discrepancy needed further investigation. We agree that this issue remains unresolved. For 22 Ronald H. Brown radiosonde profiles launched within 1 hour and 130 km of a J31 profile, comparisons of AATS and sonde LWV amounts give an r^2 of 0.90 and an RMS difference of 0.26 g/cm² (10.7%). Comparison of the corresponding J31 Vaisala and sonde values gives an r^2 of 0.92 and an RMS difference of 0.20 g/cm² (8.4%). AATS LWV retrievals are 5.5% drier than sonde values, and J31 Vaisala values are 2.3% wetter than sonde values.

[50] AATS measurements obtained during low-altitude (<120 m ASL) horizontal transects within 1 hour of satellite overpass yielded CWV retrievals in 205 MODIS IR retrieval grid cells (5 × 5-km resolution at nadir) during 5 Aqua and 5 Terra overpasses. When MODIS profile retrievals from all 10 overpasses are included in the comparison, calculated MODIS CWV values exhibit a wet bias of 0.27 g/cm² (10.4%) relative to AATS CWV, with a corresponding RMS difference of 0.54 g/cm² (21.3%). When the data are stratified by satellite, MODIS-Aqua CWV retrievals show significantly better agreement with AATS CWV than do MODIS-Terra retrievals. In particular, MODIS-Aqua values are biased wet by 0.12 g/cm² (5.1%), with an RMS difference of 0.31 g/cm² (13.7%), whereas MODIS-Terra CWV retrievals exhibit a wet bias of 0.36 g/cm² (13.2%) and an RMS difference of 0.65 g/cm² (23.8%). Our results for the ensemble are opposite those reported by *Seemann et al.* [2006] for ARM SGP “wet” (TPW ≥ 0.15 g/cm²) comparisons. They found not only that MODIS retrievals were drier than MWR measurements but also that MODIS-Terra retrievals agreed better with MWR measurements (MODIS-minus-MWR bias and RMS differences of 0.11 g/cm² and 0.32 g/cm², respectively) than did MODIS-Aqua retrievals (bias and RMS differences of 0.34 g/cm² and 0.49 g/cm², respectively). One possible explanation for the differences between the over-land [*Seemann et al.*, 2006] and over-ocean (this study) MODIS validation results is that the current MODIS retrieval algorithm partitions training data into separate land/ocean classes so no training data used over land is involved in the retrieval over ocean.

[51] In any event, examining our over-ocean results in the context of the *Seemann et al.* [2006] results obtained at the ARM SGP site leads us to conclude that additional over-ocean correlative measurement comparisons are sorely needed to understand and, hopefully, improve the behavior of the MODIS IR retrieval algorithm. In particular, the apparent difference between the MODIS-Terra and MODIS-Aqua retrievals needs to be explained. Recent improvements (S. W. Seemann et al., Development of a global infrared land surface emissivity database for application to clear sky sounding retrievals from multi-spectral satellite radiance measurements, submitted to *Journal of Applied Meteorology and Climatology*, 2007) to the MOD07 algorithm have already been implemented at the research level, and additional work on the algorithm is planned [*Seemann et al.*, 2006].

[52] The J31 flew 14 profiles within ~1.5 hours of 8 Aqua overpasses for which AIRS water vapor amounts have been retrieved. We have compared AATS and J31 Vaisala calculations of LWV with corresponding AIRS LWV retrievals, which we screened on the basis of AIRS quality control flags and on the distance from the AIRS retrieval to the J31 profile location. Specifically, results were shown for AIRS retrievals within 150 km and within 80 km of a J31 profile. We find that AIRS LWV retrievals exhibit a wet bias relative to the J31 sensor LWV values for both distance criteria, but AIRS retrievals agree better with J31 sensor values when comparisons are restricted to AIRS profiles within 80 km. In particular, for the highest-quality AIRS retrievals (*Qual_Temp_Profile_Bot* = 0), AIRS-AATS bias differences decrease from 0.19 g/cm² (8.8%) for retrievals within 150 km to 0.12 g/cm² (5.8%) for retrievals within 80 km. Corresponding AIRS-Vaisala biases decrease from 0.09 g/cm² (4.0%) to 0.02 g/cm² (1.0%). The lower AIRS-Vaisala biases compared to AIRS-AATS biases reflect the AATS 4.3% dry bias relative to the Vaisala for the subset of 14 J31 profiles included in the AIRS/J31 sensor LWV analyses. Corresponding AIRS-J31 sensor RMS differences decrease accordingly. For the highest-quality AIRS retrievals within 80 km of the AATS data, RMS differences are 0.34 g/cm² (16.4%) for AIRS-AATS and 0.28 g/cm² (12.8%) for AIRS-Vaisala.

[53] We have also compared AIRS water vapor retrievals (LWV_A) within the predefined AIRS retrieval pressure layers with corresponding AATS and J31 Vaisala retrievals calculated within those layers. AIRS profiles within 80 km of the J31 yield LWV_A retrievals that exhibit small biases compared to AATS (−2% to +6%) and Vaisala (−5% to +5%) retrievals below 700 hPa. These biases agree with the 1000–700 hPa layer biases of −4.9% to +3.1% reported by *Fetzer et al.* [2004]. They are also similar to the small AIRS wet biases of <5% reported by *Divakarla et al.* [2006] and *Tobin et al.* [2006] for 2-km layers below 400–500 hPa. The stated goal for the AIRS retrieval of water vapor concentration is 10% RMS in 2 km layers below 100 hPa [*Tobin et al.*, 2006]. AIRS-J31 sensor LWV_A relative RMS differences of ~20% below 700 hPa are consistent with the 1000–700 hPa layer values of 14–24% found by *Fetzer et al.* [2004], and with the 10–25% RMS differences (~25% for SGP data and ~10% for TWP data) reported by *Tobin et al.* [2006] below 400 hPa and the 10–30% RMS differences found by *Divakarla et al.* [2006] below 500 hPa. Above 700 hPa, AIRS-J31 sensor absolute bias and RMS differences remain small, but the magnitude and variability of the relative bias and RMS differences increase significantly and exceed the *Tobin et al.* [2006] and *Divakarla et al.* [2006] values. This behavior is attributed to the effect of spatial or temporal variability in water vapor during one or more J31 profiles on the J31 retrievals and, subsequently, on the calculated relative differences.

[54] We certainly believe that our study has provided new and useful correlative measurement results for assessing the performance of the current operational MODIS and AIRS water vapor retrieval algorithms, and we plan to conduct similar comparisons in future field campaigns. We have demonstrated how differences with AIRS data increase systematically with displacement, suggesting real variability in the satellite observations. We have also constrained the

uncertainties on satellite retrievals for midlatitude ocean conditions, and shown general consistency with other studies. These insights into the satellite observations can only be attained through careful comparisons with in situ observations, showing the value of even limited field studies.

[55] **Acknowledgments.** This research is a contribution to the International Consortium for Atmospheric Research on Transport and Transformation (ICARTT), which includes Phase A of the Intercontinental Chemical Transport Experiment (INTEX-A) of NASA and the Intercontinental Transport and Chemical Transformation (ITCT) experiment of NOAA. The AATS-14 measurements were supported by NOAA's Atmospheric Composition and Climate Program and by NASA's Programs in Radiation Science, Suborbital Science, and Tropospheric Chemistry. The analyses were supported by NASA's Earth Observing System Inter-Disciplinary Science (EOS-IDS) Program.

References

- Aumann, H. H., et al. (2003), AIRS/AMSU/HSB on the Aqua mission: Design, science objectives, data products, and processing system, *IEEE Trans. Geosci. Remote Sens.*, *41*, 253–264.
- Beer, R. (2006), TES on the Aura Mission: Scientific objectives, measurements, and analysis overview, *IEEE Trans. Geosci. Remote Sens.*, *44*, 1102–1105.
- Bögel, W. (1977), Neue Näherungsgleichungen für den Sättigungsdruck des Wasserdampfes und für die in der Meteorologie gebräuchlichen Luftfeuchte-Parameter, *DLR-FB 77-52*, Dtsch. Forsch.-und Versuchsanst. für Luft-und Raumfahrt, Oberpfaffenhofen, Germany.
- Bruegge, C. J., J. E. Conel, R. O. Green, J. S. Margolis, R. G. Holm, and G. Toon (1992), Water vapor column abundance retrievals during FIFE, *J. Geophys. Res.*, *97*, 18,759–18,768.
- Bucholtz, A. (1995), Rayleigh-scattering calculations for the terrestrial atmosphere, *Appl. Opt.*, *34*, 2765–2773.
- Clough, S. A., M. W. Shephard, E. J. Mlawer, J. S. Delamere, M. J. Iacono, K. Cady-Pereira, S. Boukabara, and P. D. Brown (2005), Atmospheric radiative transfer modeling: A summary of the AER codes, *J. Quant. Spectrosc. Radiat. Transfer*, *91*, 233–244.
- Diner, D. J., et al. (1998), Multiangle Imaging Spectroradiometer (MISR) description and experiment overview, *IEEE Trans. Geosci. Remote Sens.*, *36*, 1072–1087.
- Divakarla, M. G., C. D. Barnet, M. D. Goldberg, L. M. McMillin, E. Maddy, W. Wolf, L. Zhou, and X. Liu (2006), Validation of Atmospheric Infrared Sounder temperature and water vapor retrievals with matched radiosonde measurements and forecasts, *J. Geophys. Res.*, *111*, D09S15, doi:10.1029/2005JD006116.
- Fehsenfeld, F. C., et al. (2006), International Consortium for Atmospheric Research on Transport and Transformation (ICARTT): North America to Europe—Overview of the 2004 summer field study, *J. Geophys. Res.*, *111*, D23S01, doi:10.1029/2006JD007829.
- Fetzer, E. J., et al. (2003), Validation of AIRS/AMSU/HSB core products for data release version 3.0, August 13, 2003, *JPL D-26538*, 79 pp., NASA Goddard Space Flight Cent., Greenbelt, Md. (Available at <http://disc.gsfc.nasa.gov/AIRS/index.shtml/>)
- Fetzer, E. J., J. Teixeira, E. T. Olsen, and E. F. Fishbein (2004), Satellite remote sounding of atmospheric boundary layer temperature inversions over the subtropical eastern Pacific, *Geophys. Res. Lett.*, *31*, L17102, doi:10.1029/2004GL020174.
- Fetzer, E. J., B. H. Lambrigtsen, A. Eldering, H. H. Aumann, and M. T. Chahine (2006), Biases in total precipitable water vapor climatologies from Atmospheric Infrared Sounder and Advanced Microwave Scanning Radiometer, *J. Geophys. Res.*, *111*, D09S16, doi:10.1029/2005JD006598.
- Gao, B. C., and Y. J. Kaufman (2003), Water vapor retrievals using Moderate Resolution Imaging Spectroradiometer (MODIS) near-infrared channels, *J. Geophys. Res.*, *108*(D13), 4389, doi:10.1029/2002JD003023.
- Gettelman, A., et al. (2004), Validation of satellite data in the upper troposphere and lower stratosphere with in-situ aircraft instruments, *Geophys. Res. Lett.*, *31*, L22107, doi:10.1029/2004GL020730.
- Holben, B. N., et al. (1998), AERONET—A federated instrument network and data archive for aerosol characterization, *Remote Sens. Environ.*, *66*, 1–16.
- Hubanks, P. (2005), MODIS Atmosphere QA Plan for Collection 005, version 3.0, June 2005, NASA Goddard Space Flight Cent., Greenbelt, Md. (Available at http://modis-atmos.gsfc.nasa.gov/_docs/QA_Plan_2006_10_30.pdf)
- Ingold, T., B. Schmid, C. Mätzler, P. Demoulin, and N. Kämpfer (2000), Modeled and empirical approaches for retrieving columnar water vapor from solar transmittance measurements in the 0.72, 0.82, and 0.94 μm absorption bands, *J. Geophys. Res.*, *105*(D19), 24,327–24,344.
- Kaufman, Y. J., D. Tanré, L. A. Remer, E. Vermote, A. Chu, and B. N. Holben (1997), Operational remote sensing of tropospheric aerosol over land from EOS moderate resolution imaging spectroradiometer, *J. Geophys. Res.*, *102*, 17,051–17,067.
- King, M. D., Y. J. Kaufman, W. P. Menzel, and D. Tanre (1992), Remote sensing of cloud, aerosol, and water vapor properties from the Moderate Resolution Imaging Spectrometer (MODIS), *IEEE Trans. Geosci. Remote Sens.*, *30*, 2–27.
- Lambrigtsen, B. H. (2003), Calibration of the AIRS microwave instruments, *IEEE Trans. Geosci. Remote Sens.*, *41*, 369–378.
- Lambrigtsen, B. H., and R. V. Calheiros (2003), The humidity sounder for Brazil—An international partnership, *IEEE Trans. Geosci. Remote Sens.*, *41*, 352–361.
- Livingston, J. M., et al. (2005), Retrieval of ozone column content from airborne Sun photometer measurements during SOLVE II: Comparison with coincident satellite and aircraft measurements, *Atmos. Chem. Phys.*, *5*, 1–20.
- Martonchik, J. V., D. J. Diner, R. Kahn, M. M. Verstraete, B. Pinty, H. R. Gordon, and T. P. Ackerman (1998), Techniques for the retrieval of aerosol properties over land and ocean using multiangle imaging, *IEEE Trans. Geosci. Remote Sens.*, *36*, 1212–1227.
- Michalsky, J. J., J. C. Liljegren, and L. C. Harrison (1995), A comparison of Sun photometer derivations of total column water vapor and ozone to standard measures of same at the Southern Great Plains Atmospheric Radiation Measurement site, *J. Geophys. Res.*, *100*, 25,995–26,003.
- Miloshevich, L., H. Vomel, D. Whiteman, B. Lesht, F. Schmidlin, and F. Russo (2006), Absolute accuracy of water vapor measurement from six operational radiosonde types launched during AWEX-G and implications for AIRS validation, *J. Geophys. Res.*, *111*, D09S10, doi:10.1029/2005JD006083.
- Olsen, E. T., et al. (Ed.) (2005a), AIRS/AMSU/HSB version 4.0 data release user guide, Jet Propul. Lab., Calif. Inst. of Technol., Pasadena.
- Olsen, E. T., E. Fishbein, S.-Y. Lee, and E. Manning (Ed.) (2005b), AIRS/AMSU/HSB version 4.0 level 2 product levels and layers, Jet Propul. Lab., Calif. Inst. of Technol., Pasadena.
- Pagano, T. S., H. H. Aumann, D. E. Hagan, and K. Overoye (2003), Pre-launch and in-flight radiometric calibration of the Atmospheric Infrared Sounder (AIRS), *IEEE Trans. Geosci. Remote Sens.*, *41*, 265–273.
- Reagan, J., K. Thome, B. Herman, R. Stone, J. Deluisi, and J. Snider (1995), A comparison of columnar water-vapor retrievals obtained with near-IR solar radiometer and microwave radiometer measurements, *J. Appl. Meteorol.*, *34*, 1384–1391.
- Redemann, J., S. Masonis, B. Schmid, T. Anderson, P. Russell, J. Livingston, O. Dubovik, and A. Clarke (2003), Clear-column closure studies of aerosols and water vapor aboard the NCAR C-130 in ACE-Asia, 2001, *J. Geophys. Res.*, *108*(D23), 8655, doi:10.1029/2003JD003442.
- Redemann, J., P. Pilewskie, P. B. Russell, J. M. Livingston, S. Howard, B. Schmid, J. Pommier, W. Gore, J. Eilers, and M. Wendisch (2006), Airborne measurements of spectral direct aerosol radiative forcing in the Intercontinental chemical Transport Experiment/Intercontinental Transport and Chemical Transformation of anthropogenic pollution, 2004, *J. Geophys. Res.*, *111*, D14210, doi:10.1029/2005JD006812.
- Russell, P. B., et al. (1993a), Pinatubo and pre-Pinatubo optical-depth spectra: Mauna Loa measurements, comparisons, inferred particle size distributions, radiative effects, and relationship to lidar data, *J. Geophys. Res.*, *98*, 22,969–22,985.
- Russell, P. B., et al. (1993b), Post-Pinatubo optical depth spectra vs. latitude and vortex structure: Airborne tracking sunphotometer measurements in AAASE II, *Geophys. Res. Lett.*, *20*, 2571–2574.
- Russell, P. B., et al. (2007), Multi-grid-cell validation of satellite aerosol property retrievals in INTEX/ITCT/ICARTT 2004, *J. Geophys. Res.*, doi:10.1029/2006JD007606, in press.
- Schmid, B., and C. Wehrli (1995), Comparison of sun photometer calibration by Langley technique and standard lamp, *Appl. Opt.*, *34*, 4500–4512.
- Schmid, B., K. J. Thome, P. Demoulin, R. Peter, C. Matzler, and J. Sekler (1996), Comparison of modeled and empirical approaches for retrieving columnar water vapor from solar transmittance measurements in the 0.94- μm region, *J. Geophys. Res.*, *101*, 9345–9358.
- Schmid, B., P. R. Spyak, S. F. Biggar, C. Wehrli, J. Sekler, T. Ingold, C. Mätzler, and N. Kämpfer (1998), Evaluation of the applicability of solar and lamp radiometric calibrations of a precision Sun photometer operating between 300 and 1025 nm, *Appl. Opt.*, *37*, 3923–3941.
- Schmid, B., et al. (2000), Clear sky closure studies of lower tropospheric aerosol and water vapor during ACE 2 using airborne sunphotometer, airborne in-situ, space-borne, and ground-based measurements, *Tellus, Ser. B*, *52*, 568–593.

- Schmid, B., et al. (2001), Comparison of columnar water-vapor measurements from solar transmittance methods, *Appl. Opt.*, *40*, 1886–1896.
- Schmid, B., et al. (2003a), Coordinated airborne, spaceborne, and ground-based measurements of massive, thick aerosol layers during the dry season in Southern Africa, *J. Geophys. Res.*, *108*(D13), 8496, doi:10.1029/2002JD002297.
- Schmid, B., et al. (2003b), Column closure studies of lower tropospheric aerosol and water vapor during ACE-Asia using airborne Sun photometer and airborne in situ and ship-based lidar measurements, *J. Geophys. Res.*, *108*(D23), 8656, doi:10.1029/2002JD003361.
- Schmid, B., et al. (2006), How well do state-of-the-art techniques measuring the vertical profile of tropospheric aerosol extinction compare?, *J. Geophys. Res.*, *111*, D05S07, doi:10.1029/2005JD005837.
- Seemann, S. W., J. Li, W. P. Menzel, and L. E. Gumley (2003), Operational retrieval of atmospheric temperature, moisture, and ozone from MODIS infrared radiances, *J. Appl. Meteorol.*, *42*, 1072–1091.
- Seemann, S. W., E. E. Borbas, J. Li, W. P. Menzel, and L. E. Gumley (2006), MODIS Atmospheric Profile Retrieval Algorithm Theoretical Basis Document, NASA Goddard Space Flight Cent., Greenbelt, Md. (Available at http://modis.gsfc.nasa.gov/data/atbd/atbd_mod07.pdf)
- Singh, H. B., W. H. Brune, J. H. Crawford, D. J. Jacob, and P. B. Russell (2006), Overview of the summer 2004 Intercontinental Chemical Transport Experiment–North America (INTEX-A), *J. Geophys. Res.*, *111*, D24S01, doi:10.1029/2006JD007905.
- Sprent, P., and G. Dolby (1980), The geometric mean functional relationship, *Biometrics*, *35*, 547–550.
- Susskind, J., C. Barnet, and J. M. Blaisdell (2003), Retrieval of atmospheric and surface parameters from AIRS/AMSU/HSB data in the presence of clouds, *IEEE Trans. Geosci. Remote Sens.*, *41*, 390–409.
- Susskind, J., C. Barnet, J. Blaisdell, L. Iredell, F. Keita, L. Kouvaris, G. Molnar, and M. Chahine (2006), Accuracy of geophysical parameters derived from Atmospheric Infrared Sounder/Advanced Microwave Sounding Unit as a function of fractional cloud cover, *J. Geophys. Res.*, *111*, D09S17, doi:10.1029/2005JD006272.
- Thompson, A. M., et al. (2007), Intercontinental Chemical Transport Experiment Ozone-sonde Network Study 2004: 1. Summertime upper troposphere/lower stratosphere ozone over northeastern North America, *J. Geophys. Res.*, doi:10.1029/2006JD007441, in press.
- Tobin, D. C., H. E. Revercomb, R. O. Knuteson, B. M. Lesht, L. L. Strow, S. E. Hannon, W. F. Feltz, L. A. Moy, E. J. Fetzer, and T. S. Cress (2006), Atmospheric Radiation Measurement site atmospheric state best estimates for Atmospheric Sounder temperature and water vapor retrieval validation, *J. Geophys. Res.*, *111*, D09S14, doi:10.1029/2005JD006103.
- Whiteman, D. N., et al. (2006), Analysis of Raman lidar and radiosonde measurements from the AWEX-G field campaign and its relation to Aqua validation, *J. Geophys. Res.*, *111*, D09S09, doi:10.1029/2005JD006429.
- York, D. (1966), Least-squares fitting of a straight line, *Can. J. Phys.*, *44*, 1079–1086.
- E. Borbas and S. W. Seemann, Cooperative Institute for Meteorological Satellite Studies, University of Wisconsin, 1225 West Dayton Street, Madison, WI 53706, USA. (evab@ssec.wisc.edu; swetzel@ssec.wisc.edu)
- J. Eilers, W. Gore, and P. B. Russell, NASA Ames Research Center, MS 245-5, Moffett Field, CA 94035-1000, USA. (jeilers@mail.arc.nasa.gov; warren.j.gore@nasa.gov; philip.b.russell@nasa.gov)
- E. J. Fetzer, Jet Propulsion Laboratory, California Institute of Technology, Pasadena, CA 91109, USA. (eric.j.fetzer@jpl.nasa.gov)
- S. Howard, J. Pommier, S. A. Ramirez, and J. Redemann, Bay Area Environmental Research Institute, 560 3rd Street West, Sonoma, CA 95476, USA. (howard@solat.arc.nasa.gov; jpommier@mail.arc.nasa.gov; s.a.ramirez@mail.arc.nasa.gov; jredemann@mail.arc.nasa.gov)
- J. M. Livingston, SRI International, 333 Ravenswood Avenue, Menlo Park, CA 94025, USA. (john.livingston@sri.com)
- B. Schmid, Pacific Northwest National Laboratory, 902 Batelle Boulevard, Richland, WA 99352, USA. (beat.schmid@pub.gov)
- A. M. Thompson, Meteorology Department, Pennsylvania State University, 503 Walker Building, University Park, PA 16802-5013, USA. (anne@met.psu.edu)
- D. E. Wolfe, Earth System Research Laboratory, NOAA, 325 Broadway, Boulder, CO 80305, USA. (daniel.wolfe@noaa.gov)